



U-Pb detrital zircon dates and source provenance analysis of Phanerozoic sequences of the Congo Basin, central Gondwana

Bastien Linol, Maarten J. de Wit, Erika Barton, Michiel C.J. de Wit, François Guillocheau

► To cite this version:

Bastien Linol, Maarten J. de Wit, Erika Barton, Michiel C.J. de Wit, François Guillocheau. U-Pb detrital zircon dates and source provenance analysis of Phanerozoic sequences of the Congo Basin, central Gondwana. *Gondwana Research*, 2016, 29 (1), pp.208-219. 10.1016/j.gr.2014.11.009 . insu-01120212

HAL Id: insu-01120212

<https://insu.hal.science/insu-01120212>

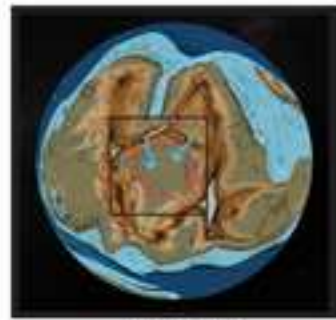
Submitted on 25 Feb 2015

HAL is a multi-disciplinary open access archive for the deposit and dissemination of scientific research documents, whether they are published or not. The documents may come from teaching and research institutions in France or abroad, or from public or private research centers.

L'archive ouverte pluridisciplinaire **HAL**, est destinée au dépôt et à la diffusion de documents scientifiques de niveau recherche, publiés ou non, émanant des établissements d'enseignement et de recherche français ou étrangers, des laboratoires publics ou privés.

*Graphical Abstract (for review)

A) Late Neoproterozoic to early Paleozoic



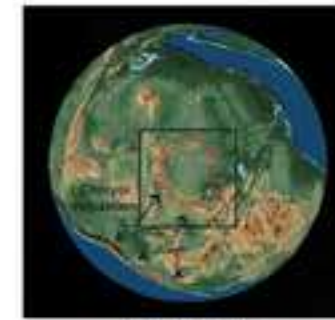
550-450 Ma

B) Carboniferous to Permian



350-300 Ma

C) Triassic



250-200 Ma

D) Late Jurassic to Early Cretaceous

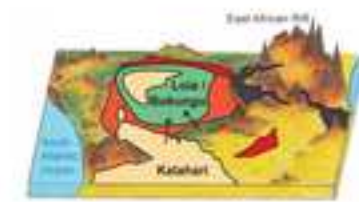
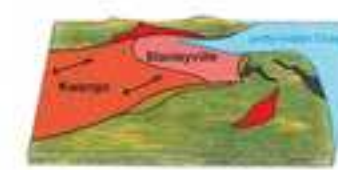


150-100 Ma

E) Mid-Cretaceous to Cenozoic



100-0 Ma



*Highlights (for review)

- A revised stratigraphy for one of the least-known large continental basins
- Track the evolution of central Gondwana via U-Pb detrital zircon geochronology
- Early Neoproterozoic (1 Ga) dates dominated in all samples

U-Pb detrital zircons dates and source provenance analysis of Phanerozoic sequences of the Congo Basin, central Gondwana

Bastien Linol^{1,2}, Maarten J. de Wit¹, Erika Barton^{1,2}, Michiel (Mike) J.C. de Wit³ and Francois Guillocheau⁴

¹ AEON-ESSRI (African Earth Observatory Network – Earth Stewardship Science Research Institute.

² Department of Geoscience, Nelson Mandela Metropolitan University, Port Elizabeth, South Africa.

Corresponding author: bastien.aeon@gmail.com

³ Delrand Resources Pty Ltd., Toronto, Ontario, Canada.

⁴ Geosciences, University of Rennes1, France.

Abstract

The Congo Basin (CB) is the largest sediment sink of central Gondwana, built on a mosaic of Precambrian crustal blocks amalgamated during the mid-Paleoproterozoic (Eburnian; 2.1-1.8 Ga), late Mesoproterozoic (Kibaran; 1.4-1.0 Ga), and late Neoproterozoic-early Cambrian (Pan African; 750-500 Ma). Sporadic uplift, tilting and erosion of these Precambrian terrains form the source regions for the sedimentary sequences that fill the CB. We investigate the Phanerozoic successions in the field and along four historic deep boreholes drilled in the center of the basin, and date detrital zircons from the main stratigraphic groups to characterize their provenance ages and reconstruct the paleogeographic evolution of the CB during amalgamation and break-up of the Gondwana supercontinent. Sedimentological data show that the oldest, upper Neoproterozoic-lower Paleozoic Redbeds (the Inkisi, Aruwimi and Biano Groups) were derived from the north. Zircons from these sequences have two dominant age-populations of 1100-950 Ma and 800-600 Ma, likely sourced from Kibaran and Pan African terrains within the Oubanguiides (e.g. the Central Saharan Belt) and parts of the North African Shield (e.g. Darfour). The overlying Carboniferous-Permian glacial and deglaciation sequences (the Lukuga Group) have similar peaks, as well as abundant zircons of 2.05-1.85 Ga and a subordinate number dated at 1.42-1.37 Ga. The latter are from Eburnian and Kibaran sources in east-central Africa, consistent with west-facing glacial paleo-valleys preserved along the

1 eastern margin of the CB. The succeeding Triassic (the Haute-Lueki Group) and
2 Jurassic-Cretaceous (the Kwango Group) fluvial and aeolian red sandstones were
3 again derived from the north. Their range of zircon dates also has two main peaks at
4 1000 Ma and 600 Ma, but also contain small younger grains of 290-240 Ma and 200-
5 190 Ma. We interpret these younger zircons to be derived from volcanic dust that
6 originated during late Paleozoic-Jurassic magmatism of the Choiyoi and Chon Aike
7 Provinces flanking the Andean subduction margin of Gondwana. By contrast, the
8 uppermost Cenozoic alluviums of the CB (the Kalahari Group) contain diamond
9 concentrates and large zircon fragments dated at 3-2.5 Ga, derived from the Kasai and
10 Cuango Cratons, to the south, which host Cretaceous diamondiferous kimberlites.
11

12
13
14
15
16
17
18
19
20 Keywords: Phanerozoic, Congo Basin, detrital zircons, sediment provenances, central
21
22
23
24
25
26
27
28
29
30
31
32
33
34
35
36
37
38
39
40
41
42
43
44
45
46
47
48
49
50
51
52
53
54
55
56
57
58
59
60
61
62
63
64
65

Keywords: Phanerozoic, Congo Basin, detrital zircons, sediment provenances, central
Gondwana.

1. Introduction

The Congo Basin (CB) is a large (ca. 1.8 million km²) Phanerozoic sedimentary basin near the center of Africa (Fig. 1) whose origin and tectonic evolution are poorly understood, mostly because of a lack of modern chronostratigraphy (Kadima et al., 2011; Sachse et al., 2012; Linol, 2013; Linol et al., 2014a, and b; de Wit and Linol, 2014). The CB was initially explored during the 1940s and 1950s, when that region, now the Democratic Republic of Congo (DRC), was part of the Belgian Congo. This early work included extensive field mapping (e.g. Robert, 1946; Cahen, 1954; Lepersonne, 1974), geophysical surveys (e.g. Jones et al., 1959; Evrard, 1960), and the drilling and coring of two deep boreholes (each ca. 2 km deep), named Samba and Dekese (Cahen et al., 1959, and 1960). These holes represent unique stratigraphic sections through the center of the basin and are now archived at the Royal Museum for Central Africa (RMCA) in Tervuren (Belgium). In the 1970s, after independence, petroleum exploration companies acquired new seismic reflection data along 36 profiles, and drilled two more (non-cored) deep boreholes, the Gilson-1 and Mbandaka-1 wells (each more than 4 km deep; EssoZaire, 1981a, and b; Lawrence and Makazu, 1988; Daly et al., 1991, and 1992). This data was used to define the geometry of main stratigraphic sequences and revealed in subsurface a series of northwest-southeast trending basement highs near the center of the basin. These highs

were interpreted to have formed as a result of far-field tectonic stresses during Neoproterozoic and late Paleozoic collision processes along Gondwana's paleo-Pacific margins (Daly et al., 1991, and 1992; Trouw and de Wit, 1999). Since these two exploration programs, very little new stratigraphic data has been acquired across the CB, hampering regional correlations and modern interpretation of its geodynamic history (Giresse, 2005; Crosby et al., 2010; Kadima et al., 2011; Buiter et al., 2012; Linol et al., 2014c).

Here, we present new U-Pb detrital zircon dates from outcrops along the Kwango River in southwestern DRC, and from selected core samples of the Samba and Dekese sections. Together with improved field, seismic and borehole stratigraphic correlations, sediment dispersal directions, and a review of dated basement rocks in and around central Africa (and central Gondwana), this source provenance analysis attempts to retrace the paleogeographic evolution of the CB during the Phanerozoic, from the time of final assembly to the break-up of the Gondwana supercontinent. Although the regional extent (one field study and two boreholes sites) and number of samples (9 samples) are limited, these U-Pb results are among the first detrital zircon dates for the CB, providing new information on the geodynamic history of interior Gondwana.

2. Geological setting

The CB is completely surrounded by Precambrian rocks, including several Archean cratonic blocks (i.e. cratons) and Proterozoic belts with regionally distinct geologic and thermo-tectonic histories, together referred to as the Central African Shield (de Wit et al., 2008; de Wit and Linol, 2014; Fig. 1A). This shield amalgamated with others continental fragments (e.g. the Kalahari and North African Shields) during the late Neoproterozoic to early Cambrian Pan African orogens (750-500 Ma; Fritz et al., 2013) to form central Gondwana, thereafter making up the foundation (i.e. crystalline basement) and providing sediments to the Phanerozoic CB (Fig. 1B).

[Figure 1 here]

Precambrian basement

The Central African Shield comprises the Kasai, NE Angola (Cuango), Ntem, Mboumou and Tanzanian Cratons (ca. 3.5-2.5 Ga; Cahen et al., 1984), surrounding

the CB (Fig. 1A). These blocks amalgamated with mid-Paleoproterozoic terrains along the Ruwenzori and Ubendian-Usagaran Belts (ca. 2.1-1.8 Ga) in Uganda and western Tanzania (Lenoir et al., 1995; Link et al., 2010; Boniface et al., 2012), the Central Angolan Mobile Belt (CAMB; ca. 2.3-2.0 Ga) in Angola (de Carvalho et al., 2000; de Wit and Linol, 2014), and the West Central African Mobile Belt (WCAMB; ca. 2.5-2.0 Ga) in western DRC, Gabon and Cameroon (Caen-Vachette et al., 1988; Feybesse et al., 1998), that extends to Transamazonian terrains in northeastern Brazil (e.g. Toteu et al., 2001; Lerouge et al., 2006; Pedrosa-Soares et al., 2008). This assemblage was subsequently affected by mid-Mesoproterozoic granitoid magmatism along the Kibaran Belt in eastern DRC, Rwanda and Burundi (ca. 1.4 Ga; Tack et al., 2010; Fernandez-Alonso et al., 2012), and again deformed during the late Mesoproterozoic to early Neoproterozoic (ca. 1 Ga) within the Oubanguiides in the Central African Republic (CAR) and Chad (e.g. the Central Saharan Belt; de Wit et al., 2014), and along the Irumide-Mozambique Belts in Zambia and northern Mozambique (Jamal, 2005; de Waele et al., 2008; Bingen et al., 2009; Roberts et al., 2012).

A Central African Shield was then finally consolidated during the Pan African along a vast system of peripheral mobile belts, folded-and-thrusted concentrically toward the proto-CB. This includes: the ca. 700-500 Ma West Congo Belt (de Carvalho et al., 2000; Tack et al., 2001; Frimmel et al., 2006; Monié et al., 2012); the Oubanguiides (ca. 850-550 Ma; Poidevin, 1985; Rolin, 1995; Toteu et al., 2006; Nkoumbou et al., 2013); the Mozambique Belt (ca. 700-550 Ma; Sommer et al., 2003; de Waele et al., 2006; Fritz et al., 2013); and the Lufilian Arc (ca. 750-550 Ma; Kampunzu and Cailteux, 1999) in southeastern DRC and northern Zambia that extends to the southwest in northern Botswana and Namibia (de Wit, 2009; Rankin et al., 2013). All these Pan African mobile belts link to a northeast- and southwest-verging thrust, or “flower structure” (the Kiri High; Daly et al., 1991, and 1992), inferred to exist beneath the center of the CB (Fig. 1A).

Phanerozoic cover of the Central African Shield

The CB preserves five main depositional successions (or “supersequences”; Linol, 2013, see also Linol et al., 2014d) ranging in age from late Neoproterozoic to Cenozoic, with a total thickness of 4-6 km near the center of the basin (Fig. 2).

[Figure 2 here]

The oldest succession, uppermost part of the Neoproterozoic to lower Paleozoic West Congo, Lindi and Katanga Supergroups (Lepersonne, 1974; Poidevin, 1985; Tack et al., 2001; Kanda et al., 2011; Tait et al., 2011), comprises about 1-1.5 km thick Redbeds, deposited regionally southward unconformably across deformed Precambrian carbonate and siliciclastic platforms that are exposed around the margins of the CB (Fig. 1B). This includes: the Aruwimi Group that outcrops abundantly south of the Oubanguiides; the Inkisi Group, east of the West Congo Belt (Alvarez et al., 1995); and the Biano Group to the north of the Lufilian Arc (Master et al., 2005). Their stratigraphy is relatively poorly constrained by field observations and geochronology, and only detrital zircons dated at 540 Ma provide a maximum early Cambrian age (Jelsma et al., 2011). Equivalent subsurface sequences of red quartzites have been proven only in the Gilson-1 and Dekese wells (Units G10 and D10; Fig. 2) in the south-central part of the basin.

A major erosion surface across the Redbeds represents a hiatus of up to 150 million years. This unconformity is overlain by Carboniferous-Permian and Triassic successions, in total between 1 km and 3 km thick, which represent the northern extensions of the Karoo Supergroup of southern Africa (e.g. Johnson et al., 1996; Catuneanu et al., 2005; Linol et al., 2014a). The lowermost parts, the Lukuga Group, are glacial and deglaciation sequences of diamictite and black shale, and sandstones with thin coal beds, dated by paleobotany from mid-Carboniferous to Late Permian (Boulouard and Calandra, 1963; Bose and Kar, 1978; Colin and Jan du Chêne, 1981). The Lukuga Group is best preserved in east-west-trending paleo-valleys along the eastern margin of the CB (Jamotte, 1932; Boutakoff, 1948; Cahen and Lepersonne, 1978; Fig. 1B), and extends in subsurface to the south-central and western parts of the basin (ca. 900 m thick at Dekese; Fig. 2). The overlying Triassic Haute Lueki Group is less precisely described in outcrop (Lombard, 1961; Bose and Kar 1976; Cahen, 1981) but, most likely is laterally equivalent to widespread arid fluvial-aeolian sequences (also “red-beds”) in south-central Africa, such as for example the Cassange Group in Angola (Antunes et al., 1990), the Lebung Group in Botswana (Bordy et al., 2010), the Omingonde Formation in Namibia (Miller, 2008), the Beaufort and Stormberg Groups in South Africa (Johnson et al., 1996; Tankard et al., 2012), and in eastern Brazil (e.g. the Santa Maria Group; Zerfass et al., 2004; Milani et al., 2007). It is between 500 m and 1800 m thick in the center of the CB (ca. 900 m at Samba; Fig. 2).

Above these sequences, and overlying a pronounced unconformity that coincides in time with the onset of break-up of Gondwana (ca. 200-160 Ma; Reeves, 1999; Jokat et al., 2003; Torsvik et al., 2012), are Upper Jurassic to Upper Cretaceous sequences of red sandstones, between 500 m and 1000 m thick, which cover the entire CB (Fig. 1B). At the base, the fluvial-deltaic Stanleyville Group intercalates in its lower part with a fossiliferous marine limestone horizon (“Lime Fine”; Cahen, 1983a) that implies a short Kimmeridgian transgression of the proto-Indian Ocean in the northeastern CB (Saint-Seine, 1955; Saint-Seine and Casier, 1962; Taverne, 1975; Giresse, 2005; Linol, 2014b). It is onlapped to the south by northeasterly-derived aeolian dunes of the Lower Kwango Group (Units D4 and G4; Fig. 2), extending continuously to the southwestern margin of the basin (Fig. 3A), and into the Paraná Basin of eastern Brazil (see Linol, 2013, and Linol et al., 2014d for details). In the center of the CB, the succeeding Loia and Bokungu Groups correspond to two superimposed lacustrine sequences (in total ca. 650 m thick at Samba; Fig. 2), both dated biostratigraphically to be Albian-Cenomanian in age (Marlière, 1950; Cox, 1960; Defrétin-Lefranc, 1967; Grékoff, 1957; Maheshwari et al., 1977; Colin, 1981; Cahen, 1983b). These sequences are overlain in the west-central part of the basin by Upper Cretaceous (also fossiliferous) fluvial red sandstones and mudstones of the Upper Kwango Group (Lepersonne, 1951; Saint Seine 1953; Grékoff, 1960; Casier, 1965; Taverne, 1976; Colin, 1994; Linol et al., 2014b).

[Figure 3 here]

The Jurassic-Cretaceous succession of the CB is in turn truncated by a peneplanation surface, covered by silcretes (“Polymorph Sandstones”; c.f. Lepersonne 1951) and alluviums of the Cenozoic Kalahari Group (Leriche, 1927; Polinard, 1932; Grékoff, 1958; de Ploey et al., 1968; Colin, 1994; e.g. Fig. 3B). This youngest sequence is between 40 m and 240 m thick in the center of the basin (Fig. 2).

3. Material and methods

Detrital zircons from nine samples, collected in the field (Fig. 3) and from the Samba and Dekese cores (Fig. 2), were U-Pb dated by Laser Ablation Multi-Collector Inductively Coupled Plasma Mass Spectrometry (LA-MC-ICP-MS; e.g. Cocherie and Robert, 2008). Together with the new sequence-stratigraphic correlations and sediment dispersal directions described above, this geochronology helps

1 understanding the evolution of source provenance ages and associated major
2 geological changes during development of the Phanerozoic CB (e.g. Fedo et al.,
3 2003).
4

5 **Core samples and preparation**
6

7 Sampling was done during fieldwork in the Kwango region of the southwest CB, and
8 while logging the Samba and Dekese sections archived at the Royal Museum for
9 Central Africa (RMCA) in Tervuren (Belgium). Two samples from outcrops and
10 seven samples from the two core-sections were analyzed (Figs. 2 and 3), representing
11 10 kg and 50 kg of red sandstones and gravels, and between 1 m and 5 m of bisected
12 core (1.5-3.5 kg each), respectively.
13

14 Heavy minerals were concentrated in the field using an Amstrong-Jig, and in
15 laboratory with the application of heavy liquid (Lithium-based Tungstate) and a
16 Frantz isodynamic separator, at the University of Cape Town (South Africa) and the
17 University of Heidelberg (Germany). The concentrates were examined under the
18 binocular microscope and for each sample between 150 and 200 zircons with different
19 size, shape, color and abundance were carefully hand-picked. Selected grains (e.g.
20 Fig. 4) were then mounted into epoxy disks, abraded down to the center of grains and
21 polished. The mounts were imaged using a JEOL microprobe in both
22 cathodoluminescence and backscatter electron modes to further characterize the
23 internal composition and structure of the zircons (e.g. zoning, inherited cores,
24 overgrowths, recrystallization and fractures). These images are also used to guide the
25 laser to specific sites during U-Pb dating (e.g. Fig. 5).
26

27 [Figure 4 here]
28

29 **Analytical method of dating**
30

31 U-Pb dating was performed in the AEON EarthLab, using a Nu Plasma HR multi-
32 collector inductively coupled plasma mass spectrometer (Nu Instruments) coupled to
33 a UP 193 solid-state laser system (New Wave Research) and a desolvation nebulizer
34 system (DSN-100, Nu Instruments). The Nu Plasma MC-ICP-MS is equipped with a
35 special collector block allowing for simultaneous detection of ion signals from masses
36 ^{238}U to ^{203}Tl . U and Tl isotopes are measured on Faraday cups, while Pb isotopes are
37 measured on ion counters. For more details see Biggin et al. (2011), and for the
38 general analytical routine Simonetti et al. (2005).
39

U and Pb data was collected in time-resolved mode including 20 s of instrument background, 20 s of gas and acid blank, and 35 s of sample ablation. The laser was operated at a repetition rate of 10 Hz and an energy density of 2-3 J/cm². The spot size varied from 15 µm to 35 µm depending on the size and on the Pb concentration of the analyzed zircon. Raw data were corrected from background signals. Mass bias correction of the ²⁰⁷Pb/²⁰⁶Pb ratio was done using the Tl-doping method of Belshaw et al. (1998). Laser-induced inter-element fractionation and time-dependent Pb/U fractionation of the ²⁰⁶Pb/²³⁸U ratio was corrected by standard bracketing of 10 unknowns, with the reference material represented by a fragment of the 611 Ma GJ1 zircon standard with an U concentration of ~ 450 ppm. ²⁰⁷Pb/²³⁵U was calculated using
$$\frac{^{207}\text{Pb}}{^{235}\text{U}} = \frac{^{207}\text{Pb}}{^{206}\text{Pb}} \times \frac{^{206}\text{Pb}}{^{238}\text{U}} \times 137.88$$
. Reported uncertainties were propagated by quadratic addition of the external reproducibility of the standard during the individual analytical session and the internal error of the respective analysis. Reported dates in this study are not common Pb corrected, since correction by the ²⁰⁴Pb method cannot be applied due to the isobaric interference of ²⁰⁴Hg, which is a contaminant of the He gas carrying the ablated material from the laser cell to the MC-ICP-MS. The accuracy of the data was checked by regular analyses of internal standards: from the Kaap Valley pluton (3227 ± 1 Ma; Kamo and Davis, 1994), and the Plešovice zircon standard (337.13 ± 0.37 Ma; Sláma et al., 2008). Concordia plots and probability diagrams were constructed using Isoplot 3.0 (Ludwig, 2003).

4. Results

In total, 568 detrital zircons were analyzed from the different stratigraphic groups (Fig. 5). The U-Pb data for each sample (between 60 and 80 analyses) are presented in Tables 1 to 9. Below, we discuss only ²⁰⁶Pb/²⁰⁷Pb dates that are concordant in the range of 90-110%, unless otherwise mentioned (for the grains younger than 500 Ma).

[Figure 5 here]

[Tables 1 to 9 about here]

Sample D1853 (the Inkisi Group)

63 analyses were performed on 60 grains in samples D1853 (Table 1) from red quartzitic sandstones of the Inkisi Group in the lower part of the Dekese section (Fig. 2). Zircons from this sample are relatively small, sub-rounded and brownish in color (Fig. 4A).

1 42 single zircon dates are concordant (in the range of 90-110%). The four oldest date
2 between 2671 ± 5 Ma and 2575 ± 9 Ma. Two zircons date at 2.0 Ga (2041 ± 7 Ma and
3 2036 ± 10 Ma), 22 date between 1107 ± 12 Ma and 881 ± 20 Ma (52%) that represent
4 the most abundant age-population, and 14 date between 835 ± 8 Ma and 609 ± 21 Ma
5 (33%). Following this distribution, the probability plot shows peaks at 2670 Ma, 2060
6 Ma, 1040 Ma and 650 Ma (Fig. 5A).
7
8
9
10

11 Samples D1400 and D1595 (the Lukuga Group)

12 In samples D1400 and D1595, from diamictites of the Lukuga Group in the middle
13 part of the Dekese section (Fig. 2), 157 analyses were performed on 148 grains
14 (Tables 2 and 3). Zircons from this group are small to large (200-500 μm), sub-
15 rounded and generally transparent (Fig. 4B).
16
17

18 In total 123 single zircon dates are concordant. The oldest zircon dates at 2925 ± 8 Ma.
19 Six zircons date between 2690 ± 16 Ma and 2428 ± 16 Ma, one dates at 2.2 Ga (2184
20 ± 16 Ma), and 41 date between 2074 ± 20 Ma and 1802 ± 12 Ma (31%) that represent
21 the most abundant age-population in the samples. Seven zircons date between 1589
22 ± 28 Ma and 1371 ± 18 Ma, 40 are between 1235 ± 9 Ma and 964 ± 20 Ma (30%), and
23 27 date between 865 ± 25 Ma and 544 ± 21 Ma (20%). The probability plot shows
24 three distinct peaks at 1930 Ma, 1040 Ma and 680 Ma (Fig. 5B).
25
26
27
28
29
30
31
32
33
34

35 Samples S1605 and S2035 (the Haute Lueki Group)

36 In samples S1605 and S2035, from red quartzitic sandstones of the Haute Lueki
37 Group in the lower part of the Samba section (Fig. 2), 124 analyses were performed
38 on 105 grains (Tables 4 and 5). Zircons from these samples are relatively small,
39 elongated and transparent or brownish in color (Fig. 4C); some have xenotime
40 overgrowths.
41
42

43 In total 56 single zircon dates are concordant. Many zircons are systematically
44 discordant due to common lead loss in the samples. The oldest zircon dates at 2470
45 ± 10 Ma; no Archean dates were found. Four zircons date between 2103 ± 5 Ma and
46 1952 ± 11 Ma, 20 date between 1094 ± 10 Ma and 899 ± 6 Ma (36%), and 31 date
47 between 794 ± 16 Ma and 579 ± 14 Ma (55%) representing the most abundant age-
48 population. The probability plot shows two major peaks at 1000 Ma and 670 Ma (Fig.
49 5C).
50
51
52
53
54
55
56
57
58
59
60
61
62
63
64
65

1
2
3
4
5
6
Samples D470, D600 and WP19 (the Lower Kwango Group)

7
8
9
10
11 In samples D470, D600 and WP19, from aeolian red sandstones of the Lower
12 Kwango Group, zircons are generally medium in size, well sorted, well rounded and
13 often transparent (Fig. 4D). Few are small, yellowish and with crystal shapes.
14

15 148 analyses were performed on 137 grains in samples D470 and D600 from the
16 upper part of the Dekese section (Tables 6 and 7). In total 94 single zircon dates are
17 concordant in these two samples. The seven oldest zircons date between 2630 ± 16 Ma
18 and 2473 ± 16 Ma, one dates at 2.1 Ga (2154 ± 16 Ma), and eight date between 2080 ± 17 Ma
19 and 1788 ± 22 Ma (8%). One zircon dates at 1.5 Ga (1548 ± 13 Ma), 27 date
20 between 1272 ± 23 Ma and 884 ± 19 Ma (29%), and 49 date between 837 ± 21 Ma and
21 513 ± 21 Ma (52%) that represent the most abundant age-population (Fig. 5D).
22 Following this distribution, the probability plot shows four peaks at 2580 Ma, 2000
23 Ma, 970 Ma and 680 Ma. The two youngest zircons have $^{206}\text{Pb}/^{238}\text{U}$ dates of 286 ± 7
24 Ma and 240 ± 6 Ma, concordant at 89% and 99%, respectively (Table 6).

25 In sample WP19, from Kwango red sandstones outcropping at a cliff near
26 Swamasangu (Fig. 3A), 66 analyses were performed on 64 grains (Table 8). 54 single
27 zircon dates are concordant. The oldest zircon dates at 3133 ± 29 Ma, four date at 2.6
28 Ga, and nine date between 2212 ± 28 Ma and 1766 ± 30 Ma (16%). 16 zircons are
29 bracketed between 1044 ± 33 Ma and 922 ± 34 Ma (28%), and 22 date between 851 ± 34 Ma
30 and 544 ± 37 Ma (41%) representing the most abundant age-population (Fig.
31 5E). One young zircon dates at 426 ± 8 Ma ($^{206}\text{Pb}/^{238}\text{U}$ date concordant at 106%), and
32 two younger $^{206}\text{Pb}/^{238}\text{U}$ date at 200 ± 10 Ma and 190 ± 10 Ma, concordant at 79% and
33 95%, respectively (Table 8).
34
35
36
37
38
39
40
41
42

43 **Sample WP103 (the Kalahari Group)**

44 Sample WP103 is taken from locally mined (diamondiferous) gravels of the Kalahari
45 Group at Kitsaku Digging in the Kwango area (Fig. 3B). In this sample, zircons are
46 coarse to very coarse (300-600 μm), both angular and well rounded, and of various
47 color (Fig. 4E). In total 50 single zircon dates are concordant (Table 9). 31 date
48 between 2958 ± 26 Ma and 2491 ± 27 Ma (62%), which represent the most abundant
49 age-population (Fig. 5F). Three zircons date between 2294 ± 29 Ma and 2158 ± 28 Ma,
50 five date at 1.9 Ga, one dates at 1.0 Ga (1058 ± 20 Ma), and nine are between 734 ± 34
51 Ma and 529 ± 36 Ma (18%). Two young zircons have $^{206}\text{Pb}/^{238}\text{U}$ dates of 300 ± 10 Ma
52 ($^{206}\text{Pb}/^{238}\text{U}$ dates concordant at 79% and 91%), and the two youngest, which are large
53
54
55
56
57
58
59
60
61
62
63
64
65

1 zircon fragments with very low U and Pb concentrations, date at 130-140 Ma
2 (concordant at 12% and 34%). The latter could represent fragments of kimberlitic
3 megacrysts but more analysis is needed to support this interpretation.
4
5
6
7

8 **5. Discussion**

9 In the different stratigraphic groups of the CB (the Inkisi, Lukuga, Haute Lueki,
10 Kwango and Kalahari Groups) four main detrital zircon age-populations are found
11 (Fig. 6A): 1) Archean to early Paleoproterozoic; 2) mid-Paleoproterozoic (Eburnian);
12 3) mid-Mesoproterozoic to early Neoproterozoic (Kibaran); and 4) late
13 Neoproterozoic to early Cambrian (Pan African), although there are differences in
14 their proportions. The occurrence of a small number (6) of Carboniferous-Jurassic
15 zircons within the uppermost Kwango and Kalahari Groups suggests the emergence
16 of younger source terrains during the late Mesozoic. This change coincides with the
17 conspicuous (break-up) unconformity at the base of the Jurassic-Cretaceous
18 succession in the CB (Fig. 2).
19
20

21 [Figure 6 here]
22
23

24 **Archean to early Paleoproterozoic (3.1 Ga and 2.9-2.4 Ga)**

25 Archean to early Paleoproterozoic dates are present in all the samples, albeit not the
26 most abundant (13% in total; Fig. 6A). The oldest zircon dates at 3.1 Ga (3133 ± 29
27 Ma), and the others range between 2959 ± 26 Ma and 2428 ± 16 Ma. These dates are
28 the most abundant in the samples from the Kwango field study area and from the
29 Dekese section (only one grain is from the Samba section). They may have been
30 derived from a number of cratonic sources surrounding the CB (Fig. 6B; see de Wit
31 and Linol, 2014, for review), for example: the ca. 2.9-2.7 Ga Kasai-Lomami and
32 Dibaya Complexes of the Kasai and Cuango Cratons (Cahen et al., 1984; Delhal,
33 1991); the 3.2-2.7 Ga Ntem Complex and Nyong Series (Caen-Vachette et al., 1988;
34 Feybesse et al., 1998; Nkoumbou et al., 2013), the 3.0-2.6 Ga Mboumou-Uganda
35 Craton (Link et al., 2010; Mänttäri et al., 2013), the Tanzanian Craton (e.g. the 3.1-2.5
36 Ga Dodoman Complex; Kabete et al. 2012; Lawley et al., 2013). Other possible
37 sources are from surrounding Proterozoic belts, such as for example from the Mbuiji-
38 Mayi and Muva sequences in southeastern DRC, which contain Archean detrital
39 zircons (Rainaud et al., 2003; Delpomdor et al., 2013). In the sample from the
40 (Kalahari) Kwango river terraces, however, the predominant dates of 2715 Ma most
41

likely correspond to migmatites and pegmatites of the Dibaya Complex (the Cuango Craton), outcropping immediately upstream along a major knickpoint, as indicated by the large size and angular shape of the zircons (Fig. 5F).

Mid-Paleoproterozoic (2.2-1.8 Ga)

Mid-Paleoproterozoic dates are represented in all the samples (18% in total; Fig. 6A), but are much more abundant in the samples from the Lukuga diamictites in the Dekese section (Fig. 5B). These dates, mainly ranging between 2.0 Ga and 1.8 Ga, correspond to widely outcropping Eburnian rock sequences in east Africa (e.g. the Toro and Ubendian Belts; Link et al., 2010; Boniface et al., 2012), as indicated by the westward direction of paleocurrents for the Lukuga Group (Fig. 6B).

Mesoproterozoic to early Neoproterozoic to (1600-850 Ma)

Mesoproterozoic to early Neoproterozoic dates are abundant in all the samples (33% in total; Fig. 6A), indicating important and prolonged contributions from Kibaran aged-terrains to the sediment sources for the CB. In the samples from the Lukuga Group five zircons dated between 1421 ± 16 Ma and 1371 ± 18 Ma. This coincides with the Kibaran-age Belt (*sensu stricto*) along the eastern margin of the basin (Fig. 6B), dated at ca. 1375 Ma (Tack et al., 2010). The lack of detrital zircons of this age (1.4 Ga) in all the other samples suggests that this large region of east-central Africa was not a major source for the CB, possibly because it was covered by later sediments or because it remained below sea level.

In all samples from all the stratigraphic sequences, most of other dates are bracketed between 1100 Ma and 950 Ma (Fig. 6A). In addition, repeated analysis on some zircons of this age also gave younger dates of 750 Ma, 700 Ma and 650 Ma, providing evidence for local recrystallization during the late Neoproterozoic. This suggests partial reworking during the Pan African orogens. Such dates are most common within the Oubanguides, in particular the ca. 1000-600 Ma Central Saharan Belt in CAR and North African Shield (e.g. in Chad; de Wit et al., 2005, and 2014; Toteu et al., in preparation), and on the South American flank of the Atlantic Ocean, especially within the Sergipano-Araguaia Belts in northeastern Brazil (e.g. dos Santos et al., 2010; de Brito Neves, 2011). These (distant) northern provenances for the CB are supported by other recent detrital zircon studies that found also dominant 1.0 Ga age-populations within the upper Neoproterozoic to lower Paleozoic West Congo and Inkisi Groups along the western margin of the basin (Frimmel et al., 2006; Jelsma et

1 al., 2011). Such Pan African metasediments and associated molasses-like basin
2 sequences, abundantly exposed around the margins of the CB, and which were
3 regionally derived from the north (Alvarez et al., 1995; Master et al., 2005; Figs. 6B
4 and 7), may also have constituted significant secondary sources for the sediments.
5
6

7 **Late Neoproterozoic to Cambrian (850-500 Ma)**

8 Late Neoproterozoic to Cambrian zircon dates are also abundant in all the samples
9 (35% in total; Fig. 6A). This series of dates, relatively continuous between 800 Ma
10 and 540 Ma, corresponds to several episodes of the Pan African orogens. However,
11 possible sources with this age-range are abundant within the Pan African mobile belts
12 that surround the CB, and at this stage it is not possible to differentiate between these
13 widely dispersed terrains. Sediment dispersal directions (Fig. 6B) favor Pan African
14 provinces located to the north (the Oubanguiides), and to the east and southeast (the
15 Mozambique and Lufilian Belts). In addition, the general increase in abundance of
16 this 850-500 Ma zircon age-population from the Paleozoic (Inkisi and Lukuga) to the
17 Mesozoic sequences (Haute Lueki and Kwango) could suggest sustained Phanerozoic
18 exhumation of the surrounding Pan African mobile belts, and/or progressive
19 concentration by recycling Paleozoic sediments (Fig. 7).

20 [Figure 7 here]

21 **Late Carboniferous-Jurassic (300-240 and 190 Ma)**

22 Six young zircons, small in size and displaying no magmatic zoning, dated at 300-240
23 Ma and 190 Ma in the Kwango and Kalahari Groups indicate some contributions from
24 Upper Carboniferous-Lower Jurassic sources to the CB. These dates may possibly
25 correspond to Permian-Triassic kimberlites and Karoo flood basalts in northern
26 Angola (Jelsma personal communication in 2011). However, it is more likely that
27 these fine and delicate zircons are related to ash fallouts linked to extensive late
28 Paleozoic-Jurassic felsic volcanism and magmatism of the Choiyoi and Chon Aike
29 Provinces in western Argentina and Chile (Mpodozis and Kay, 1992; Ramos and
30 Aleman, 2000; Munizaga et al., 2008). For instance, such air-fall tuffs are commonly
31 recorded in the Permian-Triassic sedimentary rocks of the Paraná and Karoo Basins
32 of southwestern Gondwana (Bangert et al., 1999; Guerra-Sommer et al., 2008; Milani
33 and de Wit, 2008; Fildani et al., 2009; Rocha-Campos et al., 2011). In the southern
34 CB, however, paleo-wind directions measured from the Kwango aeolianites (e.g. Fig.
35 3A) indicate strong near surface winds to the southwest. Thus, this suggests
36
37
38
39
40
41
42
43
44
45
46
47
48
49
50
51
52
53
54
55
56
57
58
59
60
61
62
63
64
65

(opposite) north-directed upper atmospheric circulations across interior Gondwana, episodically transporting volcanic dust originated from volcanoes above the Andean subduction margin of Gondwana, more than 5000 km northward to the CB (Fig. 8).

[Figure 8 here]

Conclusions

U-Pb dates from 568 detrital zircons of the Phanerozoic successions in the CB characterize the evolution of source provenances during the development of this largest basin of central Gondwana. The four main age-populations documented in this study (ca. Archean, Eburnian, Kibaran and Pan African) can be linked to potential sources within the Precambrian basement immediately surrounding the CB. An exception is a prominent peak at 950-1100 Ma (Fig. 6A), for which the most likely (larger) sources are within the Oubanguiides and the North African Shield (e.g. Darfour), and the Brasiliano Belts in northeastern Brazil, since their upper Neoproterozoic sequences and associated sedimentary cover are widespread around the CB and given that these sequences regionally derived from the north. In contrast, input from the ca. 1.4 Ga Kibaran Belt is limited to the east-derived, Carboniferous glacial deposits of the CB. This suggests that east-central Africa was mostly not a major source for the sediments, possibly because this region was covered by sediments or remained below sea-level throughout the late Paleozoic-Mesozoic, as supported by sedimentological and biostratigraphic data. In addition, some younger zircons dated at 290 Ma, 240 Ma, 200 Ma and 190 Ma in the Jurassic-Cretaceous aeolian red sandstones reflects the influence of new Permian-Jurassic sources during the Mesozoic. We interpret those to be derived from air-fall tuffs related to far-field volcanic activity of the proto-Andes flanking the southwest margin of Gondwana (Figs. 7 and 8).

Acknowledgments

We acknowledge funding through the Inkaba yeAfrica and !Khure Africa programs, supported by the DST/NRF of South Africa. We thank Max Fernandez-Alonso, Damien Delvaux and Edmond Thorose for accessing the archived cores at the Royal Museum for Central Africa (RMCA), and Ulrich Glasmacher for providing some of the zircon concentrates from the lower parts of the boreholes. B. Linol particularly

1
2
3
4
5
6
7
8
9
10
11
12
13
14
15
16
17
18
19
20
21
22
23
24
25
26
27
28
29
30
31
32
33
34
35
36
37
38
39
40
41
42
43
44
45
46
47
48
49
50
51
52
53
54
55
56
57
58
59
60
61
62
63
64
65

thanks Hielke Jelsma for discussions about the CB. We also thank S. Master and an anonymous reviewer for their comments. This is AEON contribution number 136 and Inkaba yeAfrica contribution number 115.

References

- 1 Alvarez, P., Maurin, J.C., and Vicat, J.-P., 1995. La Formation de l'Inkisi
2 (Supergroupe Ouest-congolien) en Afrique centrale (Congo et Bas-Zaire): un delta
3 d'âge Paléozoïque comblant un bassin en extension. *Journal of African Earth
4 Sciences*, 20(2), p.119-131.
- 5 Antunes, M.T., Maisey, J.G., Marques, M.M., Schaeffer, B., and Thomson, K.S.,
6 1990. Triassic fishes from the Cassange Depression (R.P. de Angola). *Universitade de
7 Lisboa, Ciencias da Terra, Numero Esp*, p.1-64.
- 8 Bangert, B., Stollhofen, H., Lorenz, V., and Armstrong, R., 1999. The
9 geochronology and significance of ash-fall tuffs in the glaciogenic Carboniferous-
10 Permian Dwyka Group of Namibia and South Africa. *Journal of African Earth
11 Sciences*, 29(1), p.33-49.
- 12 Belshaw, N.S., Freedman, P.A., O'Nions, R.K., Frank, M., and Guo, Y., 1998. A
13 new variable dispersion double-focussing plasma mass spectrometer with
14 performance illustrated for Pb isotopes. *International Journal of Mass Spectrometry*,
15 181, p.51-58.
- 16 Biggin, A.J., de Wit, M.J., Langereis, C.G., Zegers, T.E., Voûte, S., Dekkers, M.J.,
17 and Drost, K., 2011. Palaeomagnetism of Archean rocks of the Onverwacht Group,
18 Barberton Greenstone Belt (southern Africa): Evidence for a stable and potentially
19 reversing geomagnetic field at ca. 3.5 Ga. *Earth and Planetary Science Letters*, 302(3-
20 4), p.314-328.
- 21 Bingen, B., Jacobs, J., Viola, G., Henderson, I.H.C., Skår, Ø., Boyd, R., Thomas,
22 R.J., Solli, A., Key, R.M., and Daudi, E.X.F., 2009. Geochronology of the
23 Precambrian crust in the Mozambique belt in NE Mozambique, and implications for
24 Gondwana assembly. *Precambrian Research*, 170(3-4), p.231-255.
- 25 Boniface, N., Schenk, V., Appel, P. 2012. Paleoproterozoic eclogites of MORB-
26 type chemistry and three Proterozoic orogenic cycles in the Ubendian Belt
27 (Tanzania): Evidence from monazite and zircon geochronology, and geochemistry.
28 *Precambrian Research* 192-195, p.16– 33.
- 29 Bordy, E.M., Segwabe, T., and Makuke, B., 2010. Sedimentology of the Upper
30 Triassic-Lower Jurassic (?) Mosolotsane Formation (Karoo Supergroup), Kalahari
31 Karoo Basin, Botswana. *Journal of African Earth Sciences*, 58(1), p.127-140.
- 32
- 33
- 34
- 35
- 36
- 37
- 38
- 39
- 40
- 41
- 42
- 43
- 44
- 45
- 46
- 47
- 48
- 49
- 50
- 51
- 52
- 53
- 54
- 55
- 56
- 57
- 58
- 59
- 60
- 61
- 62
- 63
- 64
- 65

Bose, M.N., and Kar, R.K., 1976. Palaeozoic *sporae dispersae* from Zaïre (Congo). XI: Assises glaciaires et periglaciaire from the Lukuga Valley. Annales du Musée Royal de l'Afrique centrale, Tervuren (Belgique), Série in 8, Sciences Géologiques, 77, p.1-19.

Bose, M.N., and Kar, R.K., 1978. Biostratigraphy of the Lukuga Group in Zaire. Annales du Musée Royal de l'Afrique centrale, Tervuren (Belgique), Série in 8, Sciences Géologiques, 82, p.97-114.

Boulouard, C., and Calandra, F., 1963. Etude palynologique de quelques sondages de la République du Congo (Congo ex-Belge). Unpublished report R/ST-no.7376, SNPA Direction exploration et production Pau, France.

Boutakoff, N., 1948. Les formations glaciaires et post-glaciaires fossilifères, d'âge permo-carbonifère (Karoo inférieur) de la région de Walikale (Kivu, Congo belge). Mémoire de l'Institut géologique. Université de Louvain, IX (II), 214 pp.

Buiter, S.J.H., Steinberger, B., Medvedev, S., and Tetreault, J.L., 2012. Could the mantle have caused subsidence of the Congo Basin? *Tectonophysics*, 514-517, p.62-80.

Caen-Vachette, M., Vialette, Y., Bassot, J.-P., and Vidal, P., 1988. Apport de la géochronologie isotopique à la connaissance de la géologie gabonaise. Chroniques de la recherche minière, 491, p.35-54.

Cahen, L., 1954. Géologie du Congo Belge. Liège: Vaillant-Carmanne, 577 pp.

Cahen, L., 1981. Précisions sur la stratigraphie et les corrélations du Goupe de la Haute-Lueki et des formations comparables (Triasique à Liasique? d'Afrique Centrale). Rapport annuel du Musée Royal d'Afrique centrale, Tervuren (Belgique), Département de Géologie et de Minéralogie, p.81-96.

Cahen, L., 1983a. Le Groupe de Stanleyville (Jurassic supérieur et Wealdien de l'intérieur de la République du Zaïre): Révision des connaissances. Rapport annuel du Musée Royal de l'Afrique centrale, Tervuren (Belgique), Département de Géologie et de Minéralogie, p.73-91.

Cahen, L., 1983b. Brèves précisions sur l'âge des groupes crétaciques post-Wealdien (Loia, Bokungu, Kwango) du Bassin interieur du Congo (République du Zaïre). Rapport annuel du Musée Royal de l'Afrique centrale, Tervuren (Belgique), Département de Géologie et de Minéralogie, p.61-72.

Cahen, L., and Lepersonne, J., 1978. Synthèse des connaissances relatives au Groupe (anciennement Série) de la Lukuga (Permien du Zaïre). Annales du Musée

Royal du Congo belge, Tervuren (Belgique), Série in-8, Sciences géologiques, 82, p.115-152.

Cahen, L., Ferrand, J.J., Haarsma, M.J.F., Lepersonne, J., and Verbeek, T., 1959. Description du Sondage de Samba. Annales du Musée Royal du Congo belge, Tervuren (Belgique), Série in-8, Sciences géologiques, 29, 210p.

Cahen, L., Ferrand, J.J., Haarsma, M.J.F., Lepersonne, J., and Verbeek, T., 1960. Description du Sondage de Dekese. Annales du Musée Royal du Congo belge, Tervuren (Belgique), Série in-8, Sciences géologiques, 34, 115p.

Cahen, L., Snelling, N.J., Delhal, J., and Vail, J., 1984. The Geochronology and Evolution of Africa. Oxford: Clarendon Press, 512pp.

Casier, E., 1965, Poissons fossiles de la Série du Kwango (Congo). Annales du Musée royal de l'Afrique Centrale, Tervuren (Belgique), Série in-8, Sciences géologiques, 50, 69p.

Catuneanu, O., Wopfner, H., Eriksson, P.G., Cairncross, B., Rubidge, B.S., Smith, R.M.H., and Hancox, P.J., 2005. The Karoo basins of south-central Africa. Journal of African Earth Sciences, 43(1-3), p.211-253.

Cocherie, A., and Robert, M., 2008. Laser ablation coupled with ICP-MS applied to U-Pb zircon geochronology: A review of recent advances. Gondwana Research, 14, p.597-608.

Colin, J.-P., 1981. Paleontological study of the Esso/Texaco well Gilson-1, Zaire. Unpublished report EPR-E.WA19.81.

Colin, J.-P., 1994. Mesozoic-Cenozoic lacustrine sediments in the Zaïre Interior Basin. In: Gierlowski-Kordesch, E., and Kelts, K. (eds.), Global Geological Record of Lake Basins. Cambridge University Press, 4, pp.31-36.

Colin, J.-P., and Jan du Chêne, J., 1981. Paleontological study of the Esso/Texaco well Mbandaka-1, Zaire. Unpublished report EPR-E.WA15.81.

Cox, L.R., 1960. Further mollusca from the Lualaba beds of the Belgian Congo. Annales du Musée Royal du Congo belge, Tervuren (Belgique), 37, p.1-15.

Crosby, A. G., Fishwick, S., and White, N., 2010. Structure and evolution of the intracratonic Congo Basin. *Geochemistry Geophysics Geosystems*, 11(6), p.1-20.

Daly, M.C., Lawrence, S.R., Kimun'a, D., and Binga, M., 1991. Late Paleozoic deformation in central Africa: a result of distant collision. *Nature*, 350, p.605-607.

- Daly, M.C., Lawrence, S.R., Diemu-Tshiband, K., and Matouana, B., 1992. Tectonic evolution of the Cuvette Centrale, Zaire. *Journal of the Geological Society*, 149(4), p.539-546.
- De Brito Neves, B.B., 2011. The Paleoproterozoic in the South-American continent: Diversity in the geologic time. *Journal of South American Earth Sciences*, 32, p.270-286.
- De Carvalho, H., Tassinari, C., Alves, P.M., Guimarães, F., and Simões, M.C., 2000. Geochronological review of the Precambrian in western Angola: links with Brazil. *Journal of African Earth Sciences*, 31(2), p.383-402.
- Defretin-Lefranc, S., 1967. Étude sur les phyllopodes du Bassin du Congo. *Annales du Musée Royal de l'Afrique centrale, Tervuren (Belgique)*, Série in-8, Sciences géologiques, 56, 122p.
- Delhal, J., 1991, Situation géochronologique 1990 du Precambrian du Sud-Kasai et de l'Ouest-Shaba. *Rapport annuel du Musée Royal de l'Afrique centrale, Tervuren (Belgique)*, Département de Géologie et de Minéralogie, p.119-125.
- Delpomdor, F., Linnemann, U., Boven, A., Gärtner, A., Travin, A., Blanpied, C., Virgone, A., Jelsma, H., and Préat, A., 2013. Depositional age, provenance, and tectonic and paleoclimatic settings of the late Mesoproterozoic-middle Neoproterozoic Mbuji-Mayi Supergroup, Democratic Republic of Congo. *Palaeogeography, Palaeoclimatology, Palaeoecology*, 389, p.4-34.
- De Ploey, J., 1968. Sédimentologie et origine des sables de la série des sables ocre et de la série des ‘grès polymorphes’ (Système du Kalahari) au Congo Occidental. *Annales du Musée Royal de l'Afrique centrale, Tavuren (Belgique)*, Série in-8, Sciences géologiques, 61, 72p.
- De Waele, B., Johnson, S.P., and Pisarevsky, S.A., 2008. Palaeoproterozoic to Neoproterozoic growth and evolution of the eastern Congo Craton: Its role in the Rodinia puzzle. *Precambrian Research*, 160, p.127-141.
- De Waele, B., Liégeois, J.-P., Nemchin, A.A., and Tembo, F., 2006. Isotopic and geochemical evidence of Proterozoic episodic crustal reworking within the Irumide belt of south-central Africa, the southern metacratonic boundary of an Archaean Bangweulu Craton. *Precambrian Research*, 148(3-4), p.225-256.
- De Wit, M.J., 2009. Tsodilo Resources Limited drills extension of Zambian copper belt-like mineralization in Pan African Basement of northwest Botswana. *Tsodilo Resources Ltd. Report*. www.tsodiloresources.com

1 De Wit, M.J., Jeffery, M., Berg, H, and Nicolayson, L.O., 1988. Geological Map
2 of sectors of Gondwana re-constructed to their position ~150 Ma (with explanatory
3 notes), scale 1: 1.000.000. Tulsa: American Association of Petroleum Geologists.
4

5 De Wit, MJ, Bowring, S., Dudas, F., Kamga, G. 2005. The great Neoproterozoic
6 central Saharan arc and the amalgamation of the north African Shield. GAC-MAC-
7 CSPG-CSSS Conference, Halifax, Canada. Abstracts with programs, p43.
8

9 De Wit, M.J., de Brito Neves, B.B., Trouw, R.A.J., and Pankhurst, R.J., 2008. Pre-
10 Cenozoic correlations across the South Atlantic region: “the ties that bind”. In:
11 Pankurst, R.J., Trouw, R.A.J., Brito Neves, B.B., and de Wit, M.J. (eds.), West
12 Gondwana: Pre-Cenozoic Correlations Across the South Atlantic Region. Geological
13 Society of London, Special Publications, 294, pp.1-8.
14

15 De Wit, M.J., and Linol, B., 2014. Chapter 2: Precambrian basement of the Congo
16 Basin and its flanking terrains. In: de Wit, M.J., Guillocheau, F., and de Wit, M.J.C.
17 (Eds.), The Geology and Resource Potential of the Congo Basin, Springer-Verlag, in
18 press.
19

20 De Wit, M.J., Bowring, S., Buchwaldt, R., Dudas, F., MacPhee, D., Tagné-Kamga,
21 G., Dunn, N., Salet, A.M., and Nambatingar, D. 2014. Proterozoic crust of the Central
22 Sahara Shield. (Submitted to Gondwana Research).
23

24 Dos Santos, E.J., von Schmus, W.R.V., Kozuch, M., and Neves, B.B.D.B., 2010.
25 The Cariris Velhos tectonic event in Northeast Brazil. Journal of South American
26 Earth Sciences, 29(1), p.61-76.
27

28 Esso-Zaire SARL, 1981a. Geological Completion Report: Gilson-1. Unpublished
29 report.
30

31 Esso-Zaire SARL, 1981b. Geological Completion Report: Mbandaka-1.
32 Unpublished report.
33

34 Evrard, P., 1960. Sismique. Annales du Musée Royal du Congo belge, Tervuren
35 (Belgique), Série in-8, Sci-ences géologiques, 33, 87p.
36

37 Fedo, C.M., Sircombe, K.N., and Rainbird, R.H., 2003. Detrital zircon analysis of
38 the sedimentary record. Reviews in Mineralogy and Geochemistry, 53(1), p.277-303.
39

40 Fernandez-Alonso, A., Cutten, H., De Waele B., Tack, L., Tahon, A., Baudet, D.,
41 and Barritt, S.D., 2012. The Mesoproterozoic Karagwe-Ankole Belt (formerly the NE
42 Kibara Belt): The result of prolonged extensional intracratonic basin development
43 punctuated by two short-lived far-field compressional events. Precambrian Research,
44 216-219, p.63-86.
45

- 1 Feybesse, J.L., Johan, V., Triboulet, C., Guerrot, C. Mayaga-Mikolo, F., Bouchot,
2 V., Eko N'Dong, J., 1998. The West Central African belt: a model of 2.5-2.0 Ga
3 accretion and two-phase orogenic evolution. *Precambrian Research*, 87, p.161-216.
- 4 Fildani, A., Weislogel, A., Drinkwater, N.J., McHargue, T., Tankard, A., Wooden,
5 J., Hodgson, D., and Flint, S., 2009. U-Pb zircon ages from the southwestern Karoo
6 Basin, South Africa: Implications for the Permian-Triassic boundary. *Geology*, 37(8),
7 p.719-722.
- 8 Frimmel, H., Tack, L., Basei, M., Nutman, A, and Boven, A, 2006. Provenance
9 and chemostratigraphy of the Neoproterozoic West Congolian Group in the
10 Democratic Republic of Congo. *Journal of African Earth Sciences*, 46(3), p.221-239.
- 11 Fritz, H., Abdelsalam, M., Ali, K.A., Bingen, B., Collins, A.S., Fowler, A.R.,
12 Ghebreab, W., Hauzenberger, C.A., Johnson, P.R., Kusky, T.M., P. Macey, P., S.
13 Muhongo, S., Stern, R.J., Viola, G. 2013. Orogen styles in the East African Orogen:
14 A review of the Neoproterozoic to Cambrian tectonic evolution. *Journal of African
15 Earth Sciences*, 86, 65–106.
- 16 Giresse, P., 2005. Mesozoic-Cenozoic history of the Congo Basin. *Journal of
17 African Earth Sciences*, 43, p.301-315.
- 18 Grékoff, N., 1957. Ostracodes du Bassin du Congo. I. Jurassique supérieur et
19 Crétace inférieur du nord du basin. *Annales du Musée Royal de l'Afrique centrale*,
20 Tervuren (Belgique), Série in-8, Sciences géologiques, 19, 97p.
- 21 Grékoff, N., 1958. Ostracodes du Bassin du Congo. III. Tertiaire. *Annales du
22 Musée Royal de l'Afrique centrale*, Tervuren (Belgique), Série in-8, Sciences
23 géologiques, 22, 36p.
- 24 Grékoff, N., 1960. Ostracodes du Bassin du Congo. II. Crétacé. *Annales du Musée
25 Royal de l'Afrique centrale*, Tervuren (Belgique), Série in-8, Sciences géologiques,
26 22, 36p.
- 27 Guerra-Sommer, M., Cazzulo-Klepzig, M., Laquintinie Formoso, M.L., Menegat,
28 R., and Mendonça Fo, J.G., 2008. U-Pb dating of tonstein layers from a coal
29 succession of the southern Paraná Basin (Brazil): A new geochronological approach.
30 *Gondwana Research*, 14(3), p.474-482.
- 31 Jamal, D.L., 2005. Crustal studies across selected geotransects in NE
32 Mozambique: Differentialting between Mozambican (-Kibaran) and Pan Africa
33 events, with implications for Gondwana studies. Unpublished PhD Thesis, University
34 of Cape Town, 365 pp.
- 35
- 36
- 37
- 38
- 39
- 40
- 41
- 42
- 43
- 44
- 45
- 46
- 47
- 48
- 49
- 50
- 51
- 52
- 53
- 54
- 55
- 56
- 57
- 58
- 59
- 60
- 61
- 62
- 63
- 64
- 65

1 Jamotte, A., 1932. Contribution à l'étude géologique du basin charbonnier de la
2 Lukuga. Annales du Service des Mines, Tome II, Comité Spécial du Katanga, p.1-75.
3

4 Jelsma, H.A, Perrit, S.H., Amstrong, R., and Ferreira, H.F., 2011. Shrimp U-Pb
5 zircon geochronology of basement rocks of the Angolan Shield, western Angola.
6 Abstract, 23rd CAG, Johannesburg, 8th-14th January.
7

8 Johnson, M.R., van Vuuren, C.J., Hegenberger, W.F., Key, R., and Shoko, U.,
9 1996. The Stratigraphy of the Karoo Supergroup in southern Africa: an overview.
10 Journal of African Earth Sciences, 23(1), p.3-15.
11

12 Jokat, W., Boebel, T., König, M., and Meyer, U., 2003. Timing and geometry of
13 early Gondwana breakup. Journal of Geophysical Research: Solid Earth, 108(B9).
14

15 Jones, L., Mathieu, P.L., and Strenger, H., 1959. Magnétisme. Annales du Musée
16 Royal de l'Afrique central, Tervuren (Belgique), Série in-8, Sciences géologiques, 27,
17 30p.
18

19 Kadima, E., Delvaux, D., Sebagenzi, S.N., Tack, L., and Kabeya, S.M., 2011.
20 Structure and geological history of the Congo Basin: an integrated interpretation of
21 gravity, magnetic and reflection seismic data. Basin Research, 23(5), p.499-527.
22

23 Kamo, S.L., and Davis, D.W., 1994. Reassessment of Archean crustal
24 development in the Barberton Mountain Land, South Africa, based on U-Pb dating.
25 Tectonics, 13(1). P.167-192.
26

27 Kanda N.V., Mpiana, C., Cibambula, E., Fernandez-Alonso, M., Delvaux, D.,
28 Kadima, E., Delpomdor, F., Tahon, A., Dumont, P., Hanon, M., Baudet, D., de
29 Waele, S., and Tack, L., 2011. The 1000 m thick Redbeds sequence of the Congo
30 River Basin (CRB): a generally overlooked testimony in Central Africa of post-
31 Gondwana amalgamation (550 Ma) and pre-Karoo break-up (320 Ma). Abstract, 23rd
32 CAG, Johannesburg, 8th-14th January.
33

34 Lawley, C.J.M., Selby, D., Condon, D.J., Horstwood, M., Millar, I., Crowley, Q.,
35 Imber, J. 2013. Lithogeochemistry, geochronology and geodynamic setting of the
36 Lupa Terrane, Tanzania: Implications for the extent of the Archean Tanzanian Craton.
37 Precambrian Research, 231, p.174-193.
38

39 Lawrence, S.R., and Makazu, M.M., 1988. Zaire's Central Basin: Prospective
40 outlook. Oil & Gas Journal, 86(38), p.105-108.
41

42 Lenoir, J.L., Liegeois, J.-P., Theunissen, K., and Klerkx, J., 1995. The
43 Palaeoproterozoic Ubendian shear belt in Tanzania: geochronology and structure.
44 Journal of African Earth Sciences, 19(3), p.169-184.
45

1 Lepersonne, J., 1951. Les subdivisions du système du Karoo au Kwango (Congo
2 belge). Annales de la Société Géologique de Belgique, LXXIV, p.123-138.

3 Lepersonne, J., 1974. Carte géologique du Zaïre au 1: 2.000.000 + Notice
4 explicative. Kinshasa, République du Zaïre: Direction de la Géologie/Musée Royal de
5 l'Afrique centrale, Tervuren (Belgique).

6 Leriche, M., 1927. Les fossiles des grès polymorphes (couches de Lubilash) aux
7 confins du Congo et de l'Angola. Annales de la Société Géologique de Belgique, 50,
8 p.44-51.

9 Lerouge, C., Cocherie, A., Toteu, S.F., Penaye, J., Milési, J.-P., Tchameni, R.,
10 Nsifa, E.N., Fanning, C.M., and Deloule, E., 2006. Shrimp U-Pb zircon age evidence
11 for Paleoproterozoic sedimentation and 2.05 Ga syntectonic plutonism in the Nyong
12 Group, South-Western Cameroon: consequences for the Eburnean-Transamazonian
13 belt of NE Brazil and Central Africa. Journal of African Earth Sciences, 44(4-5),
14 p.413-427.

15 Link, K., Koehn, D., Barth, M.G., Aanyu, K., and Foley, S.F., 2010. Continuous
16 cratonic crust between the Congo and Tanzania blocks in western Uganda.
17 International Journal of Earth Sciences (Geologische Rundschau), 99, p.1559-1573.

18 Linol, B., 2013. Sedimentology and sequence stratigraphy of the Congo and
19 Kalahari Basins of south-central Africa and their evolution during the formation and
20 break-up of West Gondwana. PhD thesis, Nelson Mandela Metropolitan University,
21 375p.

22 Linol, B., de Wit, M.J., Barton, E., Guillocheau, F., de Wit, M.J.C., and Colin. J.-
23 P., 2014a. Chapter 7: Paleogeography and tectono-stratigraphy of Carboniferous-
24 Permian and Triassic 'Karoo-like' sequences of the Congo Basin. In: de Wit, M.J.,
25 Guillocheau, F., and de Wit, M.J.C. (Eds.), The Geology and Resource Potential of
26 the Congo Basin, Springer-Verlag, in press.

27 Linol, B., de Wit, M.J., Barton, E., Guillocheau, F., de Wit, M.J.C., and Colin. J.-
28 P., 2014b. Chapter 8: Facies analysis, chronostratigraphy, and paleo-environmental
29 reconstructions of the Jurassic to Cretaceous sequences of the Congo Basin. In: de
30 Wit, M.J., Guillocheau, F., and de Wit, M.J.C. (Eds.), The Geology and Resource
31 Potential of the Congo Basin, Springer-Verlag, in press.

32 Linol, B., de Wit, M.J., Guillocheau, F., Robin, C. and Dauteuil, O., 2014c.
33 Chapter 11: Multiphase Phanerozoic subsidence and uplift history recorded in the
34 Congo Basin – a complex successor basin. In: de Wit, M.J., Guillocheau, F., and de

1 Wit, M.J.C. (Eds.), The Geology and Resource Potential of the Congo Basin,
2 Springer-Verlag, in press.

3 Linol, B., de Wit, M.J., Milani, E.J., Guillocheau, F. and Scherer, C. 2014d.
4 Chapter 13: New regional correlations between the Congo, Paraná and Cape-Karoo
5 Basins of southwest Gondwana. In: de Wit, M.J., Guillocheau, F., and de Wit, M.J.C.
6 (Eds.), The Geology and Resource Potential of the Congo Basin, Springer-Verlag, in
7 press.
8

9 Lombard, A.L., 1961. La série de la Haute Lueki (partie orientale de la cuvette
10 congolaise). Bulletin de la Société belge de Géologie, de Paléontologie et
11 d'Hydrologie, 70, p.65-72.
12

13 Ludwig, K.R., 2003. Isoplot/version 3.0: A geochronological toolkit for Microsoft
14 Excel. Berkeley Geochro-nology Center Special Publication, 4, 71p.
15

16 Maheshwari, H., Bose, M.N., and Kumaran, K.P., 1977. Mesozoic *sporae*
17 *dispersae* from Zaire. II: The Loia and Bokungu Groups in the Samba borehole. III:
18 Some miospores from the Stanleyville Group. Annales du Musée Royal de l'Afrique
19 centrale, Tervuren (Belgique), Série in-8, Sciences géologiques, 80, 60p.
20

21 Marlière, R., 1950. Ostracodes et phyllopodes du système du Karoo au Congo
22 Belge. Annales du Musée du Congo belge, 6, p.1-43.
23

24 Master, S., Rainaud, C., Armstrong, R., Phillips, D., and Robb, L., 2005.
25 Provenance ages of the Neoproterozoic Katanga Supergroup (Central African
26 Copperbelt), with implications for basin evolution. Journal of African Earth Sciences,
27 42(1-5), p.41-60.
28

29 Milani, E.J., and de Wit, M.J., 2008. Correlations between the classic Paraná and
30 Cape Karoo sequences of South America and southern Africa and their basin infills
31 flanking the Gondwanides: du Toit revisited. In: Pankurst, R.J., Trouw, R.A.J., Brito
32 Neves, B.B., and de Wit, M.J. (eds.), West Gondwana: Pre-Cenozoic Correlations
33 Across the South Atlantic Region. Geological Society of London, Special
34 Publications, 294, pp.319-342.
35

36 Milani, E.J., Gonçalves de Melo, J.H., de Souza, P.A., Fernandes, L.A., and
37 França, A.B., 2007. Bacia do Paranaíba. Boletim de geociências da petrobras, 15 (2),
38 pp.265-287.
39

40 Miller, R., 2008. The Geology of Namibia, Volume 3: upper Palaeozoic-Cenozoic.
41 Windhoek, Namibia: Geological Survey.
42

43
44
45
46
47
48
49
50
51
52
53
54
55
56
57
58
59
60
61
62
63
64
65

1 Munizaga, F., Maksaev, V., Fanning, C.M., Giglio, S., Yaxley, G., and Tassinari,
2 C.C.G., 2008. Late Paleozoic-Early Triassic magmatism on the western margin of
3 Gondwana: Collahuasi area, Northern Chile. *Gondwana Research*, 13(3), p.407-427.
4

5 Nkoumbou, C., Barbey, P., Yonta-Ngouné, C., Paquette, J.L., and Villiéras, F.,
6 2013. Pre-collisional geodynamic context of the southern margin of the Pan-African
7 fold belt in Cameroon. *Journal of African Earth Sciences*,
8 10 <http://dx.doi.org/10.1016/j.jafrearsci.2013.10.002>.
9

10 Pedrosa-Soares, A.C., Alkmim, F.F., Tack, L., Noce, C.M., Babinski, M., Silva,
11 L.C., and Martins-Neto, M.A., 2008, Similarities and differences between the
12 Brazilian and African counterparts of the Neoproterozoic Araçuaí-West Congo
13 orogen. *Geological Society, London, Special Publications*, 294(1), p.153-172.
14

15 Poidevin, J.L., 1985. Le Proterozoïque supérieur de la République Centrafricaine.
16 Annales du Musée Royal de l'Afrique centrale, Tervuren (Belgique), Serie in-8,
17 Sciences Geologiques, 91, 75p.
18

19 Polinard, E., 1932. Découverte des gisements fossilifères d'eau douce sur les
20 versants de la Lubudi au Katanga méridional. *Annales de la Société Géologique de*
21 *Belgique*, 55, p.63-81.
22

23 Rainaud, C., Master, S., Armstrong, R.A. and Robb, L.J., 2003. A cryptic
24 Mesoarchaean terrane in the basement to the Central African Copperbelt. *Journal of*
25 *the Geological Society of London*, 160, p.11-14.
26

27 Ramos, V.A., and Aleman, A., 2000. Tectonic Evolution of the Andes. In:
28 Cordani, U.G., Milani, E.J., Thomaz Filho, A., and Campos, D.A. (eds.), *Tectonic*
29 *Evolution of South America*. Rio de Janeiro, Brazil: 31st international geological
30 congress, p.635-685.
31

32 Rankin, W., Webb, S.J., Kiyan, D., Kinnaird, J.A., Jones, A.G. and Evans, R.L.
33 (2013). Linking the Damara (Namibia) and Lufilian/Katangan (Zambia) belts through
34 geophysical interpretations. *Proceedings of the 13th SAGA Biennial Conference and*
35 *Exhibition*, Kruger Park, South African Geophysical Association, 4 pp.
36

37 Reeves, C.V., 1999. Aeromagnetic and gravity features of Gondwana and their
38 relation to continental break-up: more pieces, less puzzle. *Journal of African Earth*
39 *Sciences*, 28, p.263-277.
40

41 Robert, M., 1946. *Le Congo physique*. Troisième édition. Liège: H. Vaillant-
42 Carmanne, 449pp.
43

44
45
46
47
48
49
50
51
52
53
54
55
56
57
58
59
60
61
62
63
64
65

1 Rocha-Campos, A.C., Basei, M.A., Nutman, A.P., Kleiman, L.E., Varela, R.,
2 Llambias, E., Canile, F.M., and da Rosa, O.D.C.R., 2011. 30 million years of Permian
3 volcanism recorded in the Choiyoi igneous province (W Argentina) and the source for
4 younger ash fall deposits in the Paraná Basin: SHRIMP U-Pb zircon geochro-nology
5 evidence. *Gondwana Research*, 19(2), p.509-523.
6
7

8 Rolin, P., 1995. Carte tectonique de la République centrafricaine, au 1:1.500.000.
9 BRGM.
10

11 Sachse, V.F., Delvaux, D. and Littke, R., 2012. Petrological and geochemical
12 investigations of potential source rocks of the central Congo Basin, DRC. *American
13 Association of Petroleum Geologists Bulletin*, 96(2), p.245-275.
14
15

16 Saint Seine, P., 1953. Poissons de la cuvette congolaise. *Compte rendus de la
17 Société géologique de France*, 16, p.343-345.
18
19

20 Saint Seine, P., 1955. Poissons fossiles de l'étage de Stanleyville (Congo belge).
21 1^{ère} partie: La faune des argilites et schistes bitumineux. *Annales du Musée Royal de
22 l'Afrique centrale*, Tervuren (Belgique), Série in 8, Sciences Géologiques, 14, 126p.
23
24

25 Saint Seine, P., and Casier, E., 1962. Poissons fossiles des couches de Stanleyville
26 (Congo). 2^{ème} partie: La faune marine des calcaires de Songa. *Annales du Musée
27 Royal de l'Afrique centrale*, Tervuren (Belgique), Série in 8, Sciences Géologiques,
28 44, 52p.
29
30

31 Simonetti, A., Heaman, L.M., Hartlaub, R.P., Creaser, R.A., MacHattie, T.G.,
32 Böhm, C., 2005. U-Pb zircon dating by laser ablation-MC-ICP-MS using a new
33 multiple ion counting Faraday collector array. *Journal of Analytical Atomic
34 Spectrometry*, 20, p.677-686.
35
36

37 Sláma, J., Košler, J., Condon, D.J., Crowley, J.L., Gerdes, A., Hanchar, J.M.,
38 Horstwood, M.S.A., Morris, G.A., Nasdala, L., Norberg, N., Schaltegger, U.,
39 Schoene, B., Tubrett, M.N., and Whitehouse, M.J., 2008. Plešovice zircon – A new
40 natural reference material for U-Pb and Hf isotopic microanalysis. *Chemical Geology*,
41 249, p.1-35.
42
43

44 Sommer, H., Kröner, A., Hauzenberger, C., Muhongo, S., and Wingate, M.T.D.,
45 2003. Metamorphic petrology and zircon geochronology of high-grade rocks from the
46 central Mozambique Belt of Tanzania: crustal recycling of Archean and
47 Palaeoproterozoic material during the Pan-African orogeny. *Journal of Metamorphic
48 Geology*, 21, p.915-934.
49
50
51
52
53
54
55
56
57
58
59
60
61
62
63
64
65

Tack, L., Wingate, M.T.D., and Lie, J., 2001. Early Neoproterozoic magmatism (1000-910 Ma) of the Zadinian and Mayumbian Groups (Bas-Congo): onset of Rodinia rifting at the western edge of the Congo craton. *Precambrian Research*, 110, p.277-306.

Tack, L., Wingate, M.T.D., de Waele, B., Meert, J., Belousova, E., Griffin, B., Tahon, A., and Fernandez-Alonso, M., 2010. The 1375 Ma “Kibaran event” in Central Africa: Prominent emplacement of bimodal magmatism under extensional regime. *Precambrian Research*, 180(1-2), p.63-84.

Tankard, A., Welsink, H., Aukes, P., Newton, R. and Stattker, E., 2012. Chapter 23: Geodynamic interpretation of the Cape and Karoo basins, South Africa. In: Roberts, D.G. and Bally, A.W. (Eds.). *Phanerozoic Passive Margins, Cratonic Basins and Global Tectonics Maps*. Amsterdam: Elsevier. pp.869-945.

Tait, J., Delpomdor, F., Preat, A., Tack, L., Straathof, G., and Nkula, V.K., 2011. Neoproterozoic sequences of the West Congo and Lindi/Ubangi Supergroups in the Congo Craton, Central Africa. In: Arnaud, E., Halverson, G.P., and Shields-Zhou, G. (eds.), *The Geological Record of Neoproterozoic Glaciations*. Geological Society of London, Memoirs, 36, pp.185-194.

Toteu, S.F., Van Schmus, W.R., Penaye, J., and Michard, A., 2001. New U-Pb and Sm-Nd data from north-central Cameroon and its bearing on the pre-Pan African history of central Africa. *Precambrian Research*, 108(1-2), p.45-73.

Toteu, S.F., Fouateu, R.Y., Penaye, J., Tchakounte, J., Mouangue, A.C.S., van Schmus, W.R., Deloule, E., and Stendal, H., 2006. U-Pb dating of plutonic rocks involved in the nappe tectonic in southern Cameroon: consequence for the Pan-African orogenic evolution of the central African fold belt. *Journal of African Earth Sciences*, 44(4-5), p.479-493.

Taverne, L., 1975, Etude ostéologique de *Leptolepis caheni*, Téléostéen fossile du Jurassique supérieur (Kimmeridgien) de Kisangani (ex-Stanleyville, Zaïre) précédemment décrit dans le genre *Paraclupavus*. *Revue Zoologique Africaine*, 89, p.821-853.

Taverne, L., 1976, Les téléostéens fossiles du crétacé moyen de Kipala (Kwango, Zaïre). *Annales du Musée Royal de l'Afrique centrale*, Tervuren (Belgique), Série in-8, Sciences géologiques, 79, 50p.

Torsvik, T.H., van der Voo, R., Preeden, U., Mac Niocaill, C., Steinberger, B., Doubrovine, P.V., van Hinsbergen, D.J.J., Domeier, M., Gaina, C., Tohver, E., Meert,

1 J.G., McCausland, P.J.A., and Cocks, L.R., 2012. Phanerozoic Polar Wander,
2 Palaeogeography and Dynamics. *Earth Science Reviews*, 114 (3-4), p.325-368.

3 Trouw, R.A., and de Wit, M.J., 1999. Relation between the Gondwanide Orogen
4 and contemporaneous intracratonic deformation. *Journal of African Earth Sciences*,
5 28(1), p.203-213.
6

7 Zerfass, H., Chemale, F., Schultz, C.L., and Lavina, E., 2004. Tectonics and
8 sedimentation in southern South America during the Triassic. *Sedimentary Geology*,
9 166(3-4), p.265-292.
10
11
12
13
14
15
16
17
18
19
20
21
22
23
24
25
26
27
28
29
30
31
32
33
34
35
36
37
38
39
40
41
42
43
44
45
46
47
48
49
50
51
52
53
54
55
56
57
58
59
60
61
62
63
64
65

Figures

Figure 1: (A) Tectonic map of the Precambrian basement of central Gondwana (inset for location) showing the Central African Shield (dotted line), and (B) main Phanerozoic sequences of central Africa, with location of the field study area and the four deep boreholes in the CB (updated from de Wit et al., 1988, 2008, and de Wit and Linol, 2014). Red outline marks the watershed of the modern CB drainage system.

Figure 2: Borehole litho- and bio-stratigraphic correlations across the central CB (Fig. 1B for location), showing the location of core-samples with dated detrital zircons (simplified from Linol, 2013, and Linol et al., 2014a). U1, U2 and U3 mark major unconformities determined from analysis of seismic.

Figure 3: Photos of outcrops along the Kwango River, southwest DRC (Fig. 1B for location), showing the location of samples. (A) Cliff of red sandstones near Swamasangu; cross-bed sets up to 10 m thick are characteristic of Jurassic-Cretaceous aeolian dune deposits. Paleocurrent measurements ($n: 49$) indicate predominant paleo-winds blowing to the southwest and to the south (Linol, 2013; see also Linol et al., 2014b). (B) Locally mined gravels at Kitsaku infill an irregular erosion surface (dotted line) incised into Karoo (late Paleozoic) conglomerates and red siltstones.

Figure 4: Microphotographs of selected zircons collected from the Kwango field study area (WP103; Fig. 3B), and from the Samba (S) and Dekese (D) cores; sample numbers refer to depth below surface (see Fig. 2).

Figure 5: Examples of backscatter electron microprobe images (left), Concordia diagrams (middle) and frequency plots (right) of U-Pb dated detrital zircons from main Phanerozoic groups of the CB (Figs. 2 and 3 for samples location). Numbers of zircon with a distinct age-range are plotted at the top of the frequency plots.

Figure 6: (A) Frequency plot of all U-Pb single zircon dates from the CB, and (B) simplified map of Precambrian basement ages (modified from Linol, 2013 and de Wit and Linol, 2014), with main sediment dispersal directions.

Figure 7: Paleo-reconstructions (left; modified from Scotese, 2014) and schematic diagrams (right) showing the paleogeography and paleo-topographic evolution of the CB in central Gondwana. (A) Upper Neoproterozoic-lower Paleozoic Redbeds (in dark red) were regionally deposited southward between the Pan African Mountains surrounding the CB. (B) Carboniferous-Permian glacial and deglaciation sequences (in dark grey) derived from west-facing paleo-valleys incised along the eastern margin of the basin. These sequences possibly connected with the Karoo and Paraná Seas of southwestern Gondwana. (C) Triassic fluvial (aeolian?) red sandstones and siltstones (in brown) were deposited across the entire CB; but outcrops are poorly described. (D) Upper Jurassic-Lower Cretaceous fluvial-delta and aeolian sequences (in pink and pale red respectively) record a short marine transgression (from the proto-Indian Ocean) in the northeastern CB, and a paleo-desert in the southern part of the basin extending to Namibia and South America. Strong wind systems were blowing to the southwest at low latitudes across interior Gondwana. (E) Mid- Upper Cretaceous lake sequences (in green) and Cenozoic alluviums (in yellow) derived from the south, possibly related to marginal uplifts of the CB and the Kalahari epeirogeny of southern Africa.

Figure 8: Cross-section across western Gondwana (Fig. 7D for location) showing a Central Gondwana Basin flanked along its southern convergent margin by the proto-Andes. Prevailing near-surface paleo-wind directions were to the south, whilst delicate Permian-Jurassic detrital zircons originating from volcanoes along the proto-Andes imply high atmospheric flow regimes to the north into the interior of Gondwana (arrows).

Tables

Table 1: U-Pb results of detrital zircons from sample D1853 (the Inkisi Group).

Table 2: U-Pb results of detrital zircons from sample D1595 (the Lower Lukuga Group).

Table 3: U-Pb results of detrital zircons from sample D1400 (the Upper Lukuga Group).

1
2 Table 4: U-Pb results of detrital zircons from sample S2035 (the Haute Lueki Group).
3
4

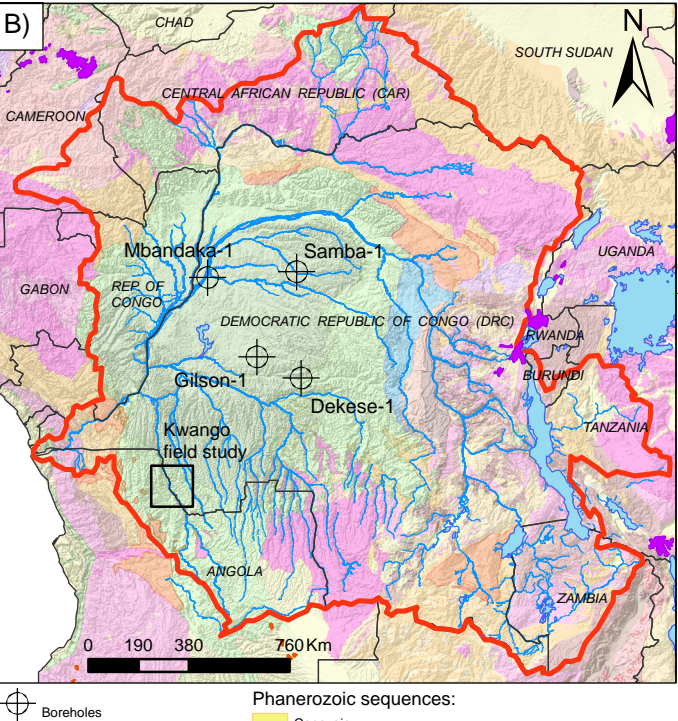
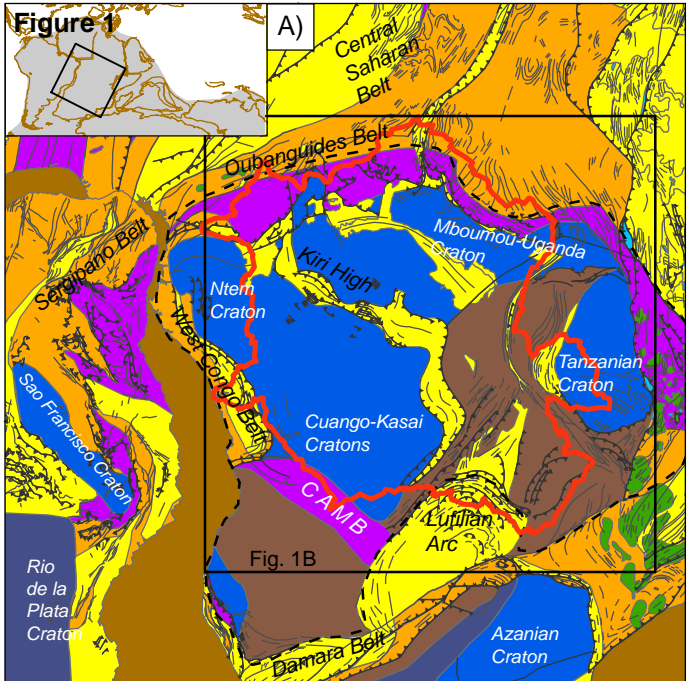
5 Table 5: U-Pb results of detrital zircons from sample S1605 (the Haute Lueki Group).
6
7

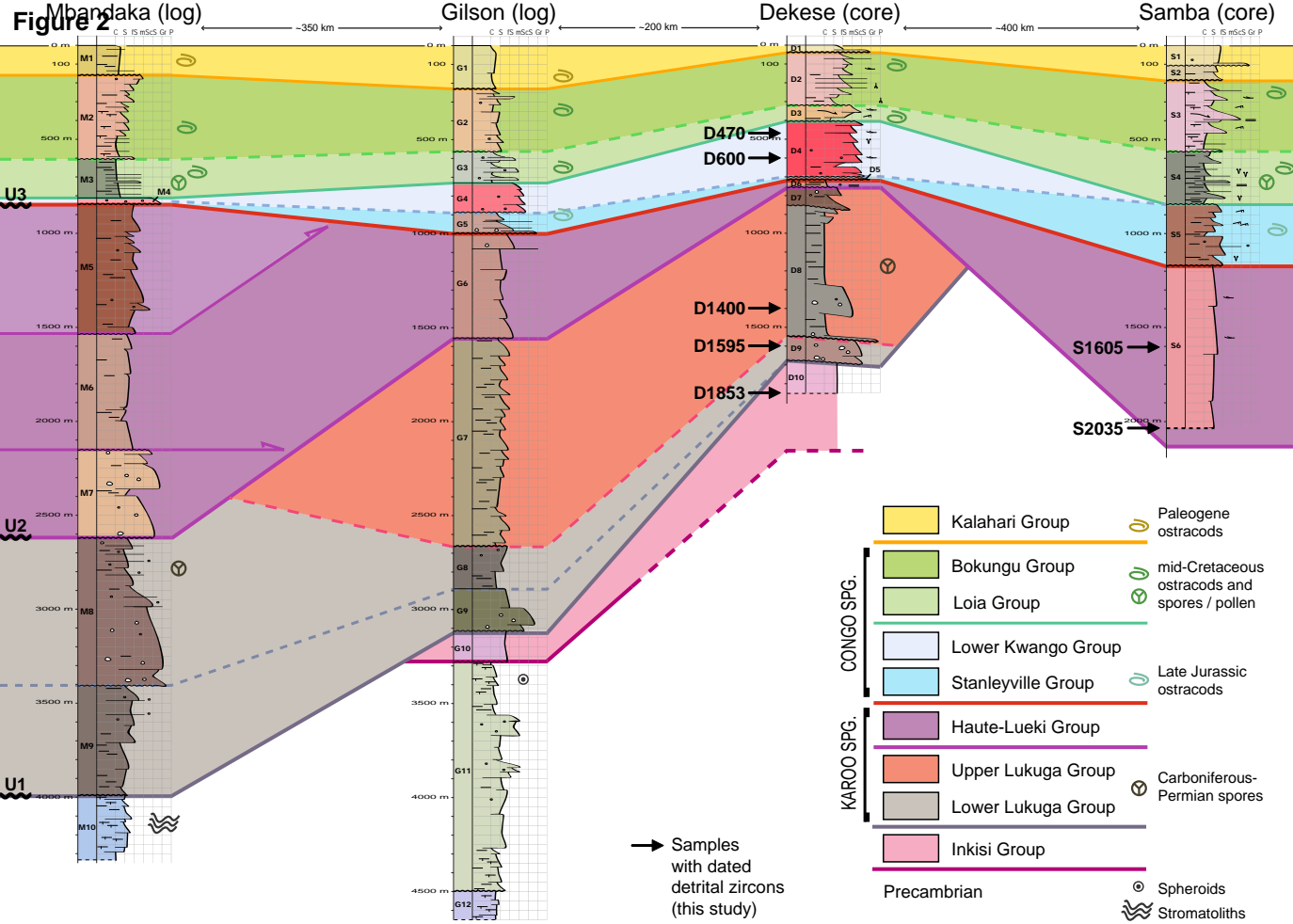
8 Table 6: U-Pb results of detrital zircons from sample D600 (the Lower Kwango
9 Group).
10
11

12 Table 7: U-Pb results of detrital zircons from sample D470 (the Lower Kwango
13 Group).
14
15

16 Table 8: U-Pb results of detrital zircons from sample WP19 (the Lower Kwango
17 Group).
18
19

20 Table 9: U-Pb results of detrital zircons from sample WP103 (the Kalahari Group).
21
22
23
24
25
26
27
28
29
30
31
32
33
34
35
36
37
38
39
40
41
42
43
44
45
46
47
48
49
50
51
52
53
54
55
56
57
58
59
60
61
62
63
64
65

Figure 1



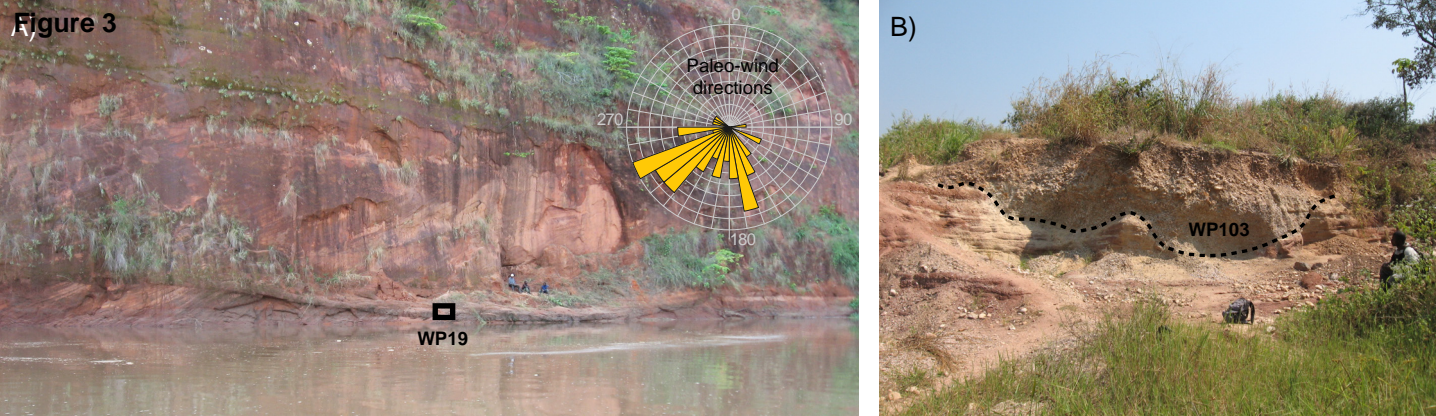


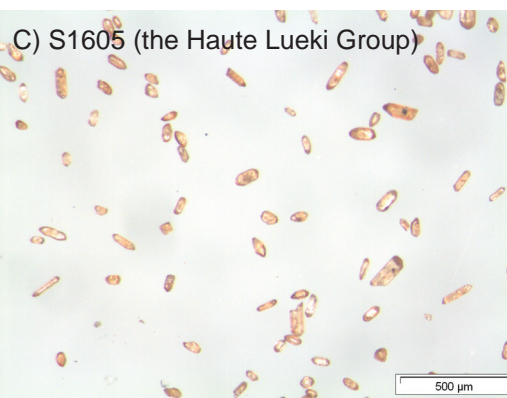
Figure 58 (the Inkisi Group)



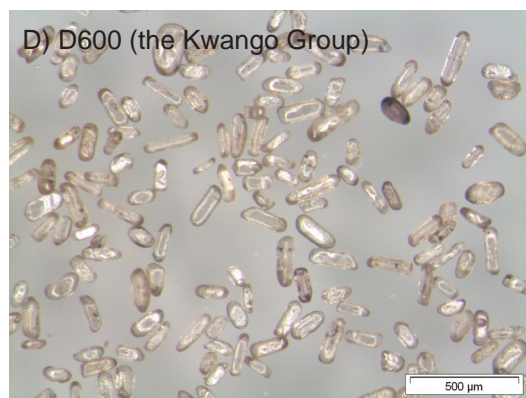
B) D1595 (the Lukuga Group)



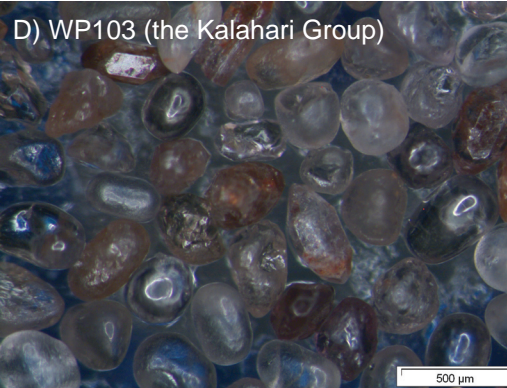
C) S1605 (the Hayte Lueki Group)



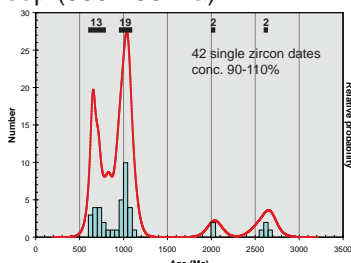
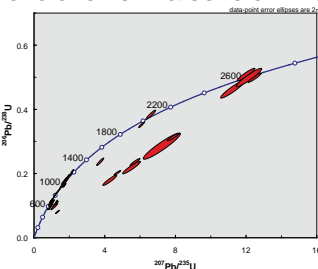
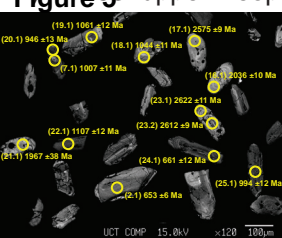
D) D600 (the Kwango Group)



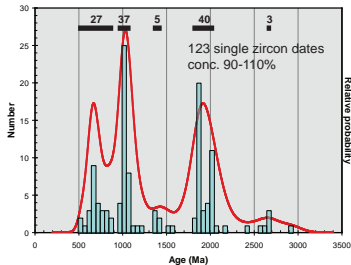
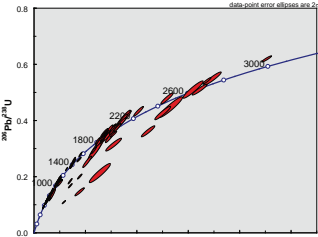
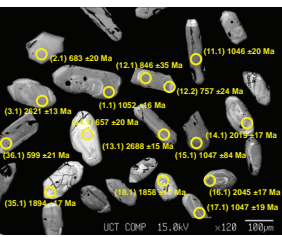
D) WP103 (the Kalahari Group)



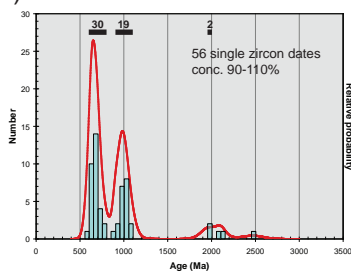
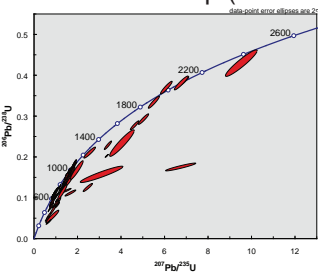
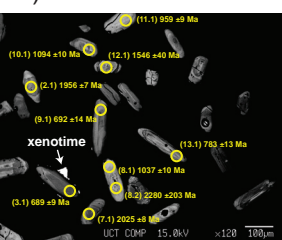
A) D1853: upper Neoproterozoic-lower Paleozoic Inkisi Group (550-450 Ma)



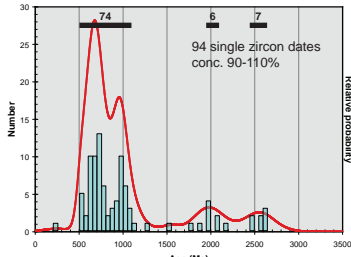
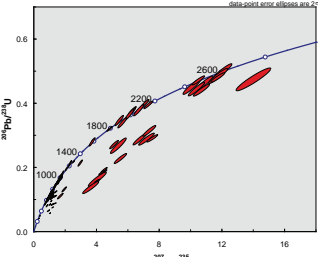
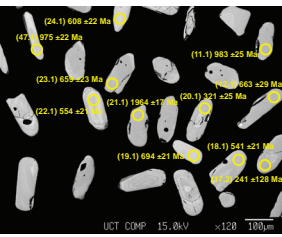
B) D1400-D1595: Carboniferous-Permian Lukuga Group (350-250 Ma)



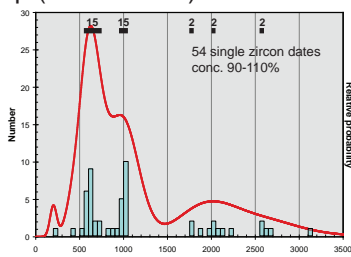
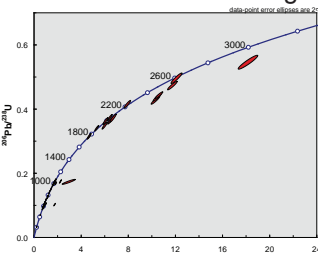
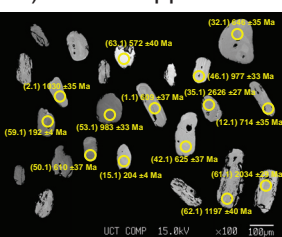
C) S1605-S2035: Triassic Haute Lueki Group (250-200 Ma)



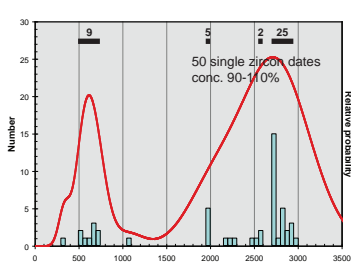
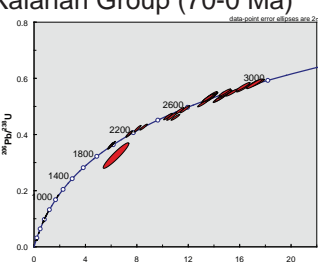
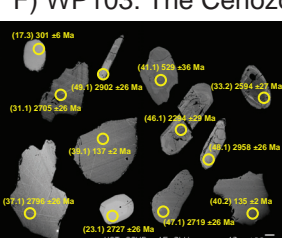
D) D470-D600: Upper Jurassic-Lower Cretaceous Kwango Group (150-100 Ma)



E) WP19: Upper Jurassic-Lower Cretaceous Kwango Group (150-100 Ma)



F) WP103: The Cenozoic Kalahari Group (70-0 Ma)



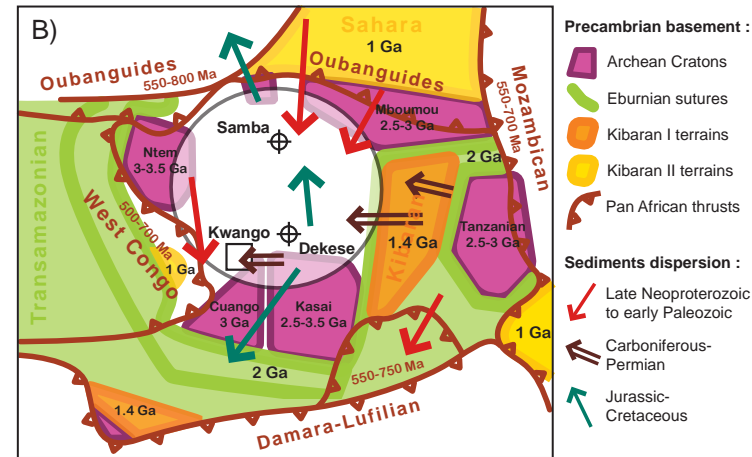
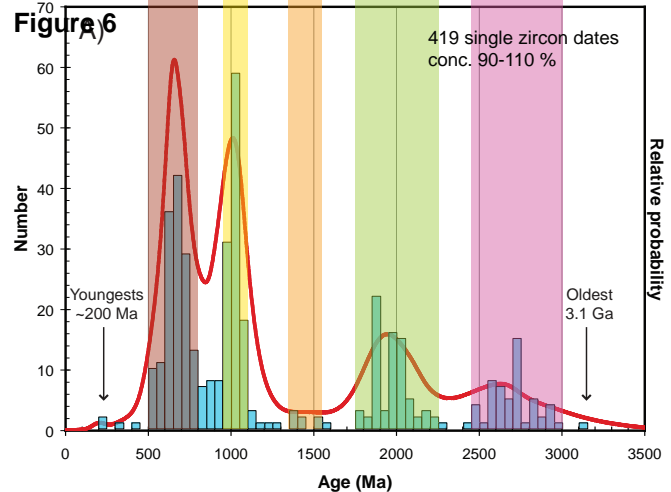
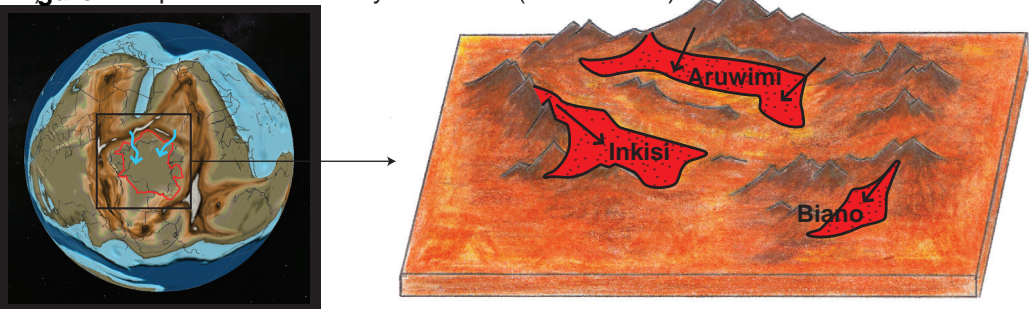
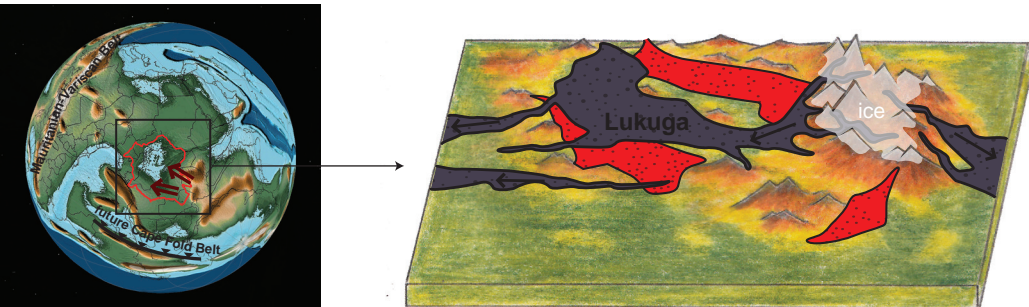


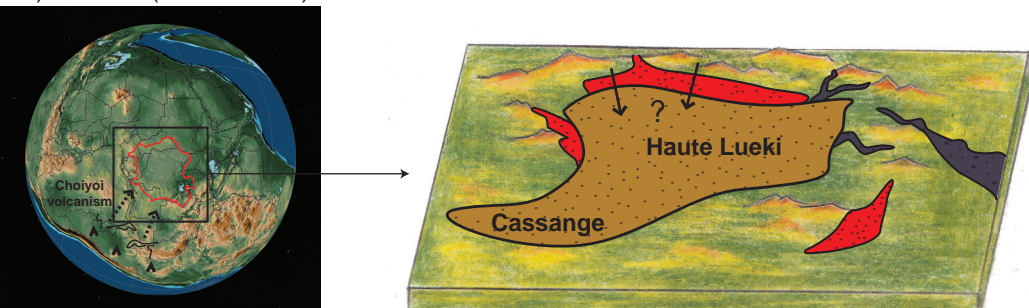
Figure 7 Neoproterozoic to early Paleozoic (550-450 Ma)



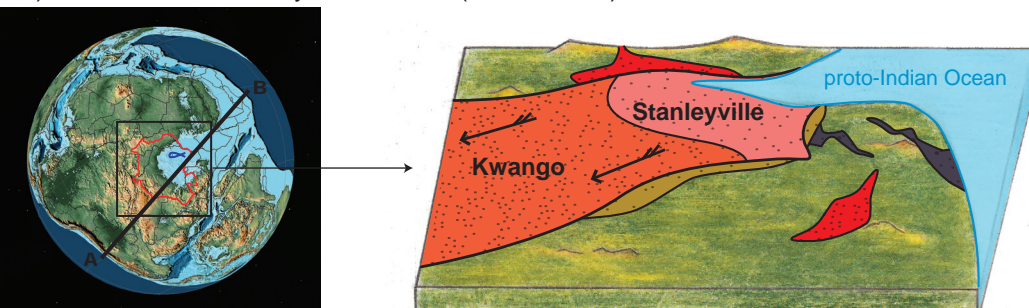
B) Carboniferous to Permian (350-300 Ma)



C) Triassic (250-200 Ma)



D) Late Jurassic to Early Cretaceous (150-100 Ma)



E) Mid-Cretaceous to Cenozoic (100-0 Ma)

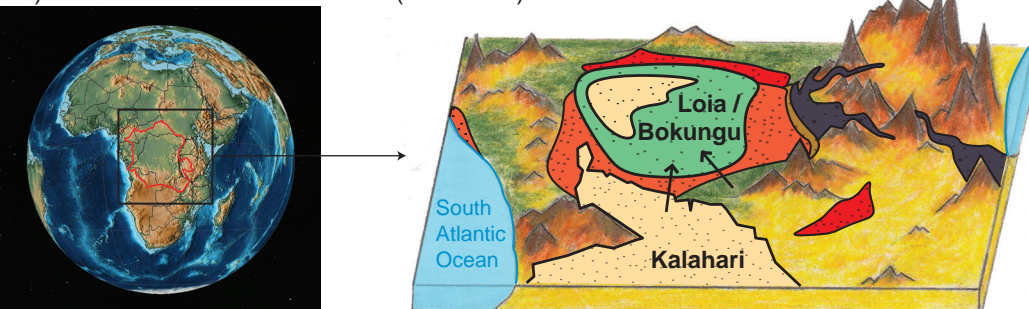


Figure 8

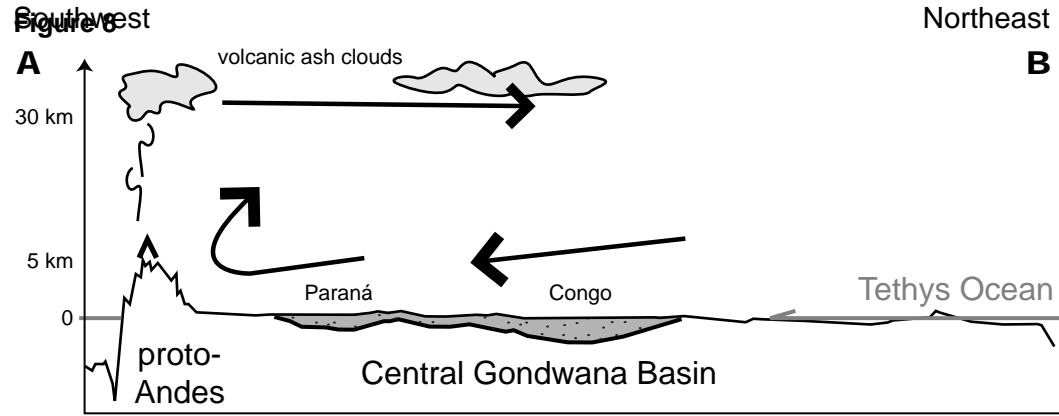


Table 1

sample	spot	U	Pb	ratios												conc.
				Ø	[ppm]	[ppm]	$^{207}\text{Pb}/^{206}\text{Pb}$	1σ	$^{207}\text{Pb}/^{235}\text{U}$	1σ	$^{206}\text{Pb}/^{238}\text{U}$	1σ	$^{207}\text{Pb}/^{206}\text{Pb}$	2σ	$^{207}\text{Pb}/^{235}\text{U}$	2σ
D11 L_1.1_10-35-55	35	2	0	0.083489	3.96	1.195708	5.18	0.10387	3.33	1281	77	799	58	637	41	50
D11 L_2.1_10-35-55	35	288	27	0.061395	0.29	0.929508	1.17	0.10980	1.14	653	6	667	12	672	14	103
D11 L_3.1_10-35-55	35	217	34	0.074285	0.31	1.834944	0.83	0.17915	0.77	1049	6	1058	11	1062	15	101
D11 L_4.1_10-35-55	35	240	77	0.125846	0.40	6.093347	1.09	0.35117	1.01	2041	7	1989	19	1940	34	95
D11 L_5.1_10-35-55	35	167	15	0.061223	0.37	0.853262	0.93	0.10108	0.85	647	8	626	9	621	10	96
D11 L_6.1_10-35-55	35	204	25	0.066915	0.37	1.271852	1.01	0.13785	0.93	835	8	833	11	833	15	100
D11 L_7.1_10-35-55	35	405	42	0.063040	0.32	1.025571	0.99	0.11799	0.94	710	7	717	10	719	13	101
D11 L_8.1_10-35-55	35	269	41	0.074121	0.31	1.747181	0.91	0.17096	0.86	1045	6	1026	12	1017	16	97
D11 L_9.1_10-35-55	35	826	120	0.075064	0.44	1.666577	1.20	0.16103	1.12	1070	9	996	15	962	20	90
D11 L_10.1_10-35-55	35	796	62	0.064085	1.15	0.773519	1.38	0.08754	0.77	744	24	582	12	541	8	73
D11 L_11.1_10-35-55	35	151	77	0.181952	0.29	12.490581	1.24	0.49788	1.21	2671	5	2642	23	2605	52	98
D11 L_12.1_10-25-55	25	195	29	0.073562	0.56	1.760987	1.82	0.17362	1.73	1029	11	1031	24	1032	33	100
D11 L_13.1_10-25-55	25	43	18	0.176928	0.56	11.267724	2.50	0.46189	2.44	2624	9	2546	47	2448	100	93
D11 L_14.1_10-25-55	25	490	98	0.115437	1.00	3.748952	2.22	0.23554	1.98	1887	18	1582	36	1363	49	72
D11 L_15.1_10-25-55	25	821	115	0.076937	0.81	1.725214	1.69	0.16263	1.48	1120	16	1018	22	971	27	87
D11 L_16.1_10-25-55	25	493	168	0.125527	0.59	6.618316	1.67	0.38239	1.57	2036	10	2062	30	2087	56	103
D11 L_17.1_10-25-55	25	263	125	0.171726	0.51	12.013340	1.67	0.50737	1.59	2575	9	2605	32	2645	69	103
D11 L_18.1_10-25-55	25	440	68	0.074093	0.56	1.850553	1.73	0.18114	1.63	1044	11	1064	23	1073	32	103
D11 L_19.1_10-25-55	25	186	29	0.074721	0.59	1.914965	2.29	0.18587	2.21	1061	12	1086	31	1099	45	104
D11 L_20.1_10-25-55	25	56	8	0.070600	0.62	1.676111	1.73	0.17219	1.62	946	13	1000	22	1024	31	108
D11 L_20.2_10-25-55	25	335	48	0.072755	0.56	1.691224	1.61	0.16859	1.51	1007	11	1005	21	1004	28	100
D11 L_21.1_10-25-55	25	1110	77	0.120742	2.13	1.311818	3.39	0.07880	2.64	1967	38	851	39	489	25	25
D11 L_22.1_10-25-55	25	58	10	0.076438	0.60	2.124907	1.98	0.20162	1.89	1107	12	1157	28	1184	41	107
D11 L_23.1_10-25-55	25	1098	245	0.176695	0.66	5.706987	2.02	0.23425	1.91	2622	11	1932	35	1357	47	52
D11 L_23.2_10-25-55	25	1819	299	0.175645	0.56	4.295603	3.74	0.17737	3.70	2612	9	1693	63	1053	72	40
D11 L_24.1_10-25-55	25	191	18	0.061629	0.58	0.934118	1.82	0.10993	1.72	661	12	670	18	672	22	102
D11 L_25.1_10-25-55	25	86	13	0.072303	0.58	1.736777	2.11	0.17421	2.03	994	12	1022	27	1035	39	104
D11 L_26.1_10-25-55	25	572	48	0.068612	4.40	0.940815	4.86	0.09945	2.07	887	91	673	48	611	24	69
D11 L_27.1_10-25-55	25	288	45	0.072089	0.53	1.763349	2.13	0.17741	2.06	988	11	1032	28	1053	40	107
D11 L_28.1_10-25-55	25	584	54	0.070794	0.84	1.068269	2.94	0.10944	2.82	951	17	738	31	670	36	70
D11 L_29.1_10-25-55	25	360	34	0.063939	1.79	0.966155	2.51	0.10959	1.75	740	38	686	25	670	22	91
D11 L_30.1_10-25-55	25	1708	454	0.184534	0.61	7.235245	5.93	0.28436	5.89	2694	10	2141	109	1613	169	60
D11 S_1.1_10-25-55	25	291	28	0.062530	0.61	0.961700	1.54	0.11155	1.42	692	13	684	15	682	18	98
D11 S_2.1_10-25-55	25	290	42	0.070956	0.64	1.606576	1.73	0.16422	1.60	956	13	973	22	980	29	103
D11 S_3.1_10-25-55	25	190	28	0.074328	1.10	1.710133	2.21	0.16687	1.92	1050	22	1012	29	995	35	95
D11 S_4.1_10-25-55	25	259	24	0.060671	0.58	0.896927	1.89	0.10722	1.80	628	13	650	18	657	23	105
D11 S_5.1_10-25-55	25	343	42	0.068411	0.97	1.343863	1.73	0.14247	1.43	881	20	865	20	859	23	97
D11 S_6.1_10-25-55	25	70	11	0.074227	0.73	1.829605	1.82	0.17877	1.67	1048	15	1056	24	1060	33	101
D11 S_7.1_10-25-55	25	502	51	0.062955	0.71	1.009572	1.63	0.11631	1.47	707	15	709	17	709	20	100
D11 S_8.1_10-25-55	25	198	22	0.065017	0.56	1.127694	1.77	0.12580	1.67	775	12	767	19	764	24	99
D11 S_9.1_10-25-55	25	491	70	0.073629	0.86	1.644191	1.72	0.16196	1.49	1031</						

Table 2

sample	spot	U	Pb	ratios												conc.
				Ø	[ppm]	[ppm]	$^{207}\text{Pb}/^{206}\text{Pb}$	1σ	$^{207}\text{Pb}/^{235}\text{U}$	1σ	$^{206}\text{Pb}/^{238}\text{U}$	1σ	$^{207}\text{Pb}/^{206}\text{Pb}$	2σ	$^{207}\text{Pb}/^{235}\text{U}$	2σ
D9 L_1.1_10-35-55	35	108	18	0.074401	0.78	1.916965	2.72	0.18687	2.61	1052	16	1087	37	1104	53	105
D9 L_2.1_10-35-55	35	185	18	0.062257	0.93	0.965333	2.63	0.11246	2.47	683	20	686	26	687	32	101
D9 L_3.1_10-35-55	35	169	82	0.176601	0.78	12.401141	2.60	0.50929	2.48	2621	13	2635	49	2654	108	101
D9 L_4.1_10-35-55	35	64	20	0.115141	0.79	5.370031	2.62	0.33826	2.49	1882	14	1880	45	1878	82	100
D9 L_5.1_10-35-55	35	180	57	0.114137	0.82	5.481889	2.71	0.34834	2.58	1866	15	1898	47	1927	86	103
D9 L_6.1_10-35-55	35	51	8	0.075506	0.87	1.877232	2.61	0.18032	2.46	1082	17	1073	35	1069	48	99
D9 L_7.1_10-35-55	35	118	12	0.062478	0.99	1.005639	2.93	0.11674	2.76	691	21	707	30	712	37	103
D9 L_8.1_10-35-55	35	249	23	0.060520	0.85	0.896393	2.63	0.10742	2.48	622	18	650	25	658	31	106
D9 L_8.2_10-35-55	35	577	55	0.061344	0.85	0.931635	2.56	0.11015	2.41	651	18	668	25	674	31	103
D9 L_9.1_10-35-55	35	142	13	0.065371	1.15	0.966952	2.90	0.10728	2.66	786	24	687	29	657	33	84
D9 L_10.1_10-25-55	25	147	23	0.074161	0.96	1.823084	1.96	0.17829	1.71	1046	19	1054	26	1058	33	101
D9 L_11.1_10-25-55	25	39	6	0.074179	1.00	1.821866	1.88	0.17813	1.59	1046	20	1053	25	1057	31	101
D9 L_12.1_10-25-55	25	77	9	0.067264	1.69	1.165765	2.49	0.12570	1.83	846	35	785	27	763	26	90
D9 L_12.2_10-15-55	25	81	9	0.064467	1.14	1.190333	2.51	0.13391	2.24	757	24	796	28	810	34	107
D9 L_13.1_10-25-55	25	171	85	0.183889	0.93	12.898897	1.82	0.50874	1.57	2688	15	2672	35	2651	68	99
D9 L_14.1_10-25-55	25	398	150	0.124333	0.94	6.920386	2.08	0.40368	1.85	2019	17	2101	37	2186	69	108
D9 L_15.1_10-25-55	25	58	7	0.074214	4.15	1.360778	4.56	0.13298	1.89	1047	84	872	54	805	29	77
D9 L_16.1_10-25-55	25	236	86	0.126160	0.96	6.830598	1.93	0.39268	1.68	2045	17	2090	34	2135	61	104
D9 L_17.1_10-25-55	25	97	16	0.074205	0.95	1.839339	1.82	0.17977	1.55	1047	19	1060	24	1066	30	102
D9 L_18.1_10-25-55	25	227	68	0.113602	0.95	5.078570	1.95	0.32423	1.70	1858	17	1833	33	1810	54	97
D9 L_19.1_10-25-55	25	109	17	0.071224	0.96	1.719401	1.93	0.17509	1.68	964	20	1016	25	1040	32	108
D9 L_20.1_10-25-55	25	141	45	0.114982	0.96	5.524330	1.85	0.34846	1.58	1880	17	1904	32	1927	53	103
D9 L_21.1_10-25-55	25	80	25	0.115614	0.97	5.350290	2.09	0.33563	1.85	1889	17	1877	36	1866	60	99
D9 L_22.1_10-25-55	25	100	31	0.115340	0.96	5.385322	2.06	0.33863	1.82	1885	17	1883	36	1880	60	100
D9 L_23.1_10-25-55	25	163	52	0.114842	0.94	5.337474	1.86	0.33708	1.60	1877	17	1875	32	1873	52	100
D9 L_24.1_10-25-55	25	694	81	0.076940	1.38	1.452036	5.66	0.13688	5.49	1120	28	911	69	827	85	74
D9 L_25.1_10-25-55	25	235	52	0.087508	0.96	2.928560	1.95	0.24272	1.69	1372	19	1389	30	1401	43	102
D9 L_26.1_10-25-55	25	450	42	0.062958	1.01	0.904598	1.87	0.10421	1.57	707	22	654	18	639	19	90
D9 L_27.1_10-25-55	25	128	40	0.116163	0.95	5.382189	1.83	0.33604	1.56	1898	17	1882	32	1868	51	98
D9 L_28.1_10-25-55	25	647	231	0.178750	0.99	8.882398	2.40	0.36040	2.18	2641	16	2326	44	1984	75	75
D9 L_29.1_10-25-55	25	176	28	0.073853	0.95	1.777801	1.88	0.17459	1.62	1037	19	1037	25	1037	31	100
D9 L_30.1_10-25-55	25	1549	295	0.129514	0.99	3.550961	2.03	0.19885	1.77	2091	17	1539	32	1169	38	56
D9 L_31.1_10-25-55	25	301	125	0.170864	1.00	10.024796	2.52	0.42552	2.32	2566	17	2437	47	2286	90	89
D9 L_32.1_10-25-55	25	127	30	0.088917	0.95	3.099945	1.83	0.25285	1.56	1402	18	1433	28	1453	41	104
D9 L_33.1_10-25-55	25	61	7	0.069118	1.29	1.188354	3.36	0.12470	3.11	902	27	795	37	758	44	84
D9 L_34.1_10-25-55	25	522	50	0.061516	0.95	0.911840	1.82	0.10750	1.56	657	20	658	18	658	20	100
D9 L_35.1_10-20-55	20	260	88	0.115926	0.94	5.836804	2.22	0.36517	2.01	1894	17	1952	39	2007	70	106
D9 L_36.1_10-25-55	25	367	32	0.059862	0.95	0.799291	1.86	0.09684	1.60	599	21	596	17	596	18	100
D9 L_37.1_10-25-55	25	2858	304	0.155640	1.09	2.317478	2.33	0.10799	2.07	2409	18	1218	33	661	26	27
D9 L_38.1_10-25-55	25	276	47	0.075958	0.96	1.938536	1.94	0.18510	1.68	1094	19	1094	26	1095	34	100
D9 L_39.1_10-25-55	25	17	3	0.073318	1.18	1.771088	2.23	0.17520	1.89	1023	24					

Table 3

sample	spot	U	Pb	ratios												conc.
				\emptyset	[ppm]	[ppm]	$^{207}\text{Pb}/^{206}\text{Pb}$	1 σ	$^{207}\text{Pb}/^{235}\text{U}$	1 σ	$^{206}\text{Pb}/^{238}\text{U}$	1 σ	$^{207}\text{Pb}/^{206}\text{Pb}$	2 σ	$^{207}\text{Pb}/^{235}\text{U}$	2 σ
D8 L_1.1_10-35-55	35	198	20	0.063052	0.74	1.065998	2.67	0.12262	2.57	710	16	737	28	746	36	105
D8 L_2.1_10-35-55	35	176	26	0.073216	0.73	1.764828	2.56	0.17482	2.45	1020	15	1033	33	1039	47	102
D8 L_3.1_10-35-55	35	706	68	0.066101	0.96	1.094903	5.01	0.12013	4.92	810	20	751	54	731	68	90
D8 L_4.1_10-35-55	35	164	26	0.074961	0.74	1.891210	2.75	0.18298	2.65	1067	15	1078	37	1083	53	101
D8 L_5.1_10-35-55	35	34	6	0.074817	0.80	1.962046	2.68	0.19020	2.55	1064	16	1103	36	1122	53	106
D8 L_6.1_10-35-55	35	183	68	0.125742	1.02	7.110912	2.62	0.41015	2.42	2039	18	2125	47	2216	91	109
D8 L_6.2_10-35-55	35	254	80	0.120812	0.73	5.764138	2.53	0.34604	2.42	1968	13	1941	44	1916	80	97
D8 L_7.1_10-35-55	35	63	10	0.073664	0.79	1.799031	2.63	0.17713	2.51	1032	16	1045	35	1051	49	102
D8 L_8.1_10-35-55	35	90	14	0.072854	0.78	1.754719	2.59	0.17469	2.47	1010	16	1029	34	1038	47	103
D8 L_9.1_10-35-55	35	319	114	0.123711	0.73	6.782288	2.56	0.39762	2.45	2010	13	2083	46	2158	90	107
D8 L_10.1_10-25-55	25	517	202	0.136585	0.93	8.127245	1.85	0.43156	1.60	2184	16	2245	34	2313	62	106
D8 L_11.1_10-25-55	25	648	145	0.086446	0.94	3.080761	1.76	0.25847	1.48	1348	18	1428	27	1482	39	110
D8 L_11.2_10-25-55	25	711	145	0.087472	0.94	2.879710	1.97	0.23877	1.73	1371	18	1377	30	1380	43	101
D8 L_12.1_10-25-55	25	538	41	0.058375	0.95	0.734784	1.88	0.09129	1.62	544	21	559	16	563	18	104
D8 L_13.1_10-25-55	25	521	178	0.125729	0.94	6.616784	1.99	0.38169	1.76	2039	17	2062	35	2084	63	102
D8 L_14.1_10-25-55	25	159	24	0.072425	0.95	1.697641	2.45	0.17000	2.26	998	19	1008	32	1012	42	101
D8 L_15.1_10-25-55	25	520	186	0.125643	0.94	6.859309	1.85	0.39595	1.60	2038	17	2093	33	2150	58	106
D8 L_16.1_10-25-55	25	198	62	0.114618	0.96	5.639805	1.95	0.35687	1.69	1874	17	1922	34	1967	58	105
D8 L_17.1_10-25-55	25	235	35	0.074025	1.03	1.766760	1.87	0.17310	1.56	1042	21	1033	24	1029	30	99
D8 L_18.1_10-25-55	25	51	16	0.111708	1.11	5.455737	2.07	0.35422	1.75	1827	20	1894	36	1955	59	107
D8 L_19.1_10-25-55	25	467	134	0.117262	1.21	5.081665	2.60	0.31430	2.30	1915	22	1833	45	1762	71	92
D8 L_20.1_10-25-55	25	173	24	0.074205	0.95	1.686175	2.16	0.16480	1.94	1047	19	1003	28	983	35	94
D8 L_21.1_10-20-55	20	2429	377	0.082753	2.93	2.009302	4.00	0.17610	2.72	1263	57	1119	55	1046	53	83
D8 L_22.1_10-20-55	20	187	17	0.060036	1.03	0.888892	2.17	0.10738	1.91	605	22	646	21	658	24	109
D8 L_23.1_10-20-55	20	1188	503	0.173013	1.12	10.650078	3.54	0.44645	3.35	2587	19	2493	67	2379	134	92
D8 L_24.1_10-25-55	25	283	44	0.073494	0.95	1.851480	1.85	0.18271	1.59	1028	19	1064	25	1082	32	105
D8 L_25.1_10-25-55	25	316	97	0.124810	0.94	6.311598	2.31	0.36677	2.10	2026	17	2020	41	2014	73	99
D8 L_26.1_10-25-55	25	113	17	0.073036	0.97	1.788823	1.95	0.17764	1.69	1015	20	1041	26	1054	33	104
D8 L_27.1_10-20-55	20	1044	401	0.124007	0.93	7.146468	2.01	0.41797	1.78	2015	17	2130	36	2251	68	112
D8 L_28.1_10-25-55	25	92	29	0.114433	0.94	5.438157	1.84	0.34467	1.58	1871	17	1891	32	1909	52	102
D8 L_29.1_10-25-55	25	186	59	0.113215	0.95	5.494212	1.87	0.35197	1.61	1852	17	1900	32	1944	54	105
D8 L_30.1_10-25-55	25	121	64	0.184043	0.97	13.907439	2.01	0.54806	1.76	2690	16	2743	38	2817	81	105
D8 L_31.1_10-25-55	25	183	27	0.071554	0.95	1.694518	1.89	0.17175	1.64	973	19	1006	24	1022	31	105
D8 L_32.1_10-25-55	25	228	77	0.119731	0.95	6.093962	1.87	0.36914	1.61	1952	17	1989	33	2025	56	104
D8 L_33.1_10-25-55	25	477	166	0.123967	0.97	6.431026	1.87	0.37625	1.59	2014	17	2037	33	2059	56	102
D8 L_34.1_10-25-55	25	135	61	0.157399	0.93	10.359344	1.93	0.47734	1.69	2428	16	2467	36	2516	71	104
D8 L_35.1_10-25-55	25	104	16	0.072627	0.97	1.807756	2.03	0.18053	1.78	1004	20	1048	27	1070	35	107
D8 L_36.1_10-20-55	20	2369	651	0.117213	0.98	4.886263	5.09	0.30234	5.00	1914	18	1800	88	1703	150	89
D8 L_36.2_10-20-55	20	1748	422	0.119142	1.15	4.702178	4.65	0.28624	4.51	1943	21	1768	79	1623	130	83
D8 S_1.1_10-25-55	25	592	69	0.065937	0.62	1.198905	1.42	0.13187	1.28	804	13	800	16	799	19	99
D8 S_2.1																

Table 4

sample	spot	U	Pb	ratios												conc.
				Ø	[ppm]	[ppm]	$^{207}\text{Pb}/^{206}\text{Pb}$	1σ	$^{207}\text{Pb}/^{235}\text{U}$	1σ	$^{206}\text{Pb}/^{238}\text{U}$	1σ	$^{207}\text{Pb}/^{206}\text{Pb}$	2σ	$^{207}\text{Pb}/^{235}\text{U}$	2σ
S10 L 1.1 10-25-55	25	1548	92	0.090611	1.27	0.876986	6.26	0.07020	6.13	1438	24	639	60	437	52	30
S10 L 1.2 10-25-55	25	1054	149	0.076974	1.60	1.774952	2.39	0.16724	1.78	1121	32	1036	31	997	33	89
S10 L 2.1 10-25-55	25	491	143	0.120003	0.40	5.511502	1.85	0.33310	1.81	1956	7	1902	32	1853	58	95
S10 L 3.1 10-25-55	25	329	31	0.062427	0.43	0.958710	1.39	0.11138	1.33	689	9	683	14	681	17	99
S10 L 3.2 10-20-55	25	61	11	0.280890	3.58	6.749587	4.22	0.17428	2.24	3368	56	2079	76	1036	43	31
S10 L 4.1 10-25-55	25	1399	110	0.081118	0.44	1.029034	1.60	0.09200	1.53	1224	9	718	17	567	17	46
S10 L 5.1 10-25-55	25	295	56	0.088777	3.40	2.567568	4.27	0.20976	2.58	1399	65	1291	63	1228	58	88
S10 L 6.1 10-25-55	25	1197	84	0.066324	0.72	0.756089	1.86	0.08268	1.72	817	15	572	16	512	17	63
S10 L 7.1 10-25-55	25	170	25	0.073387	0.41	1.745827	1.59	0.17254	1.53	1025	8	1026	21	1026	29	100
S10 L 8.1 10-25-55	25	1167	156	0.073844	0.48	1.571251	1.59	0.15432	1.52	1037	10	959	20	925	26	89
S10 L 8.2 10-20-55	25	1321	174	0.144330	11.78	3.111394	12.88	0.15635	5.20	2280	203	1436	208	936	91	41
S10 L 9.1 10-25-55	25	604	54	0.062509	0.65	0.925015	1.62	0.10733	1.48	692	14	665	16	657	19	95
S10 L 10.1 10-25-55	25	611	94	0.075954	0.49	1.875213	1.46	0.17906	1.38	1094	10	1072	19	1062	27	97
S10 L 11.1 10-25-55	25	874	123	0.071042	0.46	1.586280	2.27	0.16194	2.22	959	9	965	28	968	40	101
S10 L 12.1 10-25-55	25	1656	117	0.095904	2.12	1.071488	3.72	0.08103	3.06	1546	40	739	39	502	30	32
S10 L 13.1 10-25-55	25	913	79	0.065281	0.61	0.916682	1.59	0.10184	1.47	783	13	661	16	625	18	80
S10 L 14.1 10-25-55	25	734	103	0.071039	0.38	1.617237	1.43	0.16511	1.37	959	8	977	18	985	25	103
S10 L 15.1 10-25-55	25	602	81	0.070386	0.45	1.512715	1.20	0.15587	1.12	940	9	936	15	934	19	99
S10 L 16.1 10-25-55	25	296	43	0.072672	1.30	1.678859	1.79	0.16755	1.23	1005	26	1001	23	999	23	99
S10 L 16.2 10-25-55	25	627	127	0.108310	0.86	3.397139	2.06	0.22748	1.87	1771	16	1504	33	1321	45	75
S10 L 17.1 10-25-55	25	1669	122	0.069036	0.73	0.826738	2.27	0.08685	2.15	900	15	612	21	537	22	60
S10 L 18.1 10-25-55	25	881	73	0.064348	0.38	0.859518	1.29	0.09688	1.23	753	8	630	12	596	14	79
S10 L 18.2 10-20-55	25	2542	94	0.114913	7.32	0.842923	13.98	0.05320	11.91	1879	132	621	134	334	78	18
S10 L 19.1 10-25-55	25	709	62	0.065639	1.71	0.921313	2.79	0.10180	2.20	795	36	663	27	625	26	79
S10 L 19.2 10-25-55	25	469	40	0.063097	0.65	0.846206	1.69	0.09727	1.56	711	14	623	16	598	18	84
S10 L 20.1 10-25-55	25	839	110	0.070880	0.57	1.472928	1.44	0.15072	1.32	954	12	919	18	905	22	95
S10 L 21.1 10-25-55	25	829	109	0.071597	0.58	1.519822	3.07	0.15396	3.02	974	12	938	38	923	52	95
S10 L 22.1 10-25-55	25	959	65	0.073163	1.81	0.797571	4.68	0.07906	4.32	1018	37	595	43	491	41	48
S10 L 23.1 10-25-55	25	2521	86	0.122222	2.56	0.640217	5.28	0.03799	4.62	1989	46	502	42	240	22	12
S10 S_1.1_10-25-55	25	1465	153	0.077599	0.62	1.307860	2.31	0.12224	2.23	1137	12	849	27	743	31	65
S10 S_2.1_10-25-55	25	382	37	0.063415	0.61	0.997329	2.05	0.11406	1.95	722	13	702	21	696	26	96
S10 S_3.1_10-25-55	25	687	52	0.067563	1.38	0.851736	4.24	0.09143	4.01	855	29	626	40	564	43	66
S10 S_4.1_10-25-55	25	215	33	0.073490	0.58	1.768238	2.11	0.17451	2.03	1027	12	1034	28	1037	39	101
S10 S_5.1_10-25-55	25	1328	172	0.074902	0.73	1.575857	1.88	0.15259	1.74	1066	15	961	24	915	30	86
S10 S_6.1_10-25-55	25	411	63	0.073127	0.62	1.810898	1.76	0.17960	1.65	1017	13	1049	23	1065	32	105
S10 S_7.1_10-25-55	25	3252	121	0.123776	1.25	0.708929	3.34	0.04154	3.09	2011	22	544	28	262	16	13
S10 S_8.1_10-25-55	25	1468	393	0.125244	0.64	5.042121	1.91	0.29198	1.80	2032	11	1826	33	1651	52	81
S10 S_8.2_10-25-55	25	611	213	0.129270	0.61	6.781080	1.93	0.38045	1.83	2088	11	2083	34	2078	65	100
S10 S_9.1_10-25-55	25	432	68	0.072965	0.57	1.854578	1.88	0.18434	1.79	1013	12	1065	25	1091	36	108
S10 S_10.1_10-25-55	25	254	23	0.061148	0.65	0.931817	1.81	0.11052	1.68	644	14	669	18	676	22	105
S10 S_10.2_10-25-55	25	115	11	0.061634	0.69	0.935554	1.80	0.11009	1.66	6						

Table 5

sample	spot	U	Pb	ratios												conc.
				Ø	[ppm]	[ppm]	$^{207}\text{Pb}/^{206}\text{Pb}$	1σ	$^{207}\text{Pb}/^{235}\text{U}$	1σ	$^{206}\text{Pb}/^{238}\text{U}$	1σ	$^{207}\text{Pb}/^{206}\text{Pb}$	2σ	$^{207}\text{Pb}/^{235}\text{U}$	2σ
S8 L_1.1_10-35-55	35	731	63	0.062131	0.30	0.882789	0.83	0.10305	0.78	679	6	642	8	632	9	93
S8 L_1.2_10-35-55	35	308	28	0.060269	0.67	0.875916	1.94	0.10541	1.82	613	14	639	18	646	22	105
S8 L_2.1_10-35-55	35	955	129	0.080402	0.63	1.778234	2.15	0.16041	2.06	1207	12	1038	28	959	37	79
S8 L_3.1_10-35-55	35	272	25	0.065632	0.86	1.005293	1.60	0.11109	1.35	795	18	706	16	679	17	85
S8 L_4.1_10-35-55	35	353	64	0.120373	0.39	3.342706	0.83	0.20140	0.74	1962	7	1491	13	1183	16	60
S8 L_4.2_10-25-55	25	509	202	0.161342	0.58	9.542483	3.13	0.42896	3.07	2470	10	2392	58	2301	120	93
S8 L_5.1_10-35-55	35	314	27	0.062969	0.40	0.885584	1.01	0.10200	0.93	707	8	644	10	626	11	89
S8 L_6.1_10-35-55	35	321	28	0.064164	0.47	0.897184	1.21	0.10141	1.12	747	10	650	12	623	13	83
S8 L_7.1_10-35-55	35	224	32	0.072794	0.40	1.673689	0.88	0.16675	0.78	1008	8	999	11	994	14	99
S8 L_8.1_10-35-55	35	181	64	0.130352	0.29	6.938641	1.05	0.38606	1.01	2103	5	2104	19	2105	36	100
S8 L_9.1_10-35-55	35	525	71	0.069021	0.28	1.471451	0.89	0.15462	0.84	899	6	919	11	927	15	103
S8 L_10.1_10-35-55	35	119	11	0.060762	0.34	0.866531	1.20	0.10343	1.15	631	7	634	11	634	14	101
S8 L_11.1_10-25-55	25	216	19	0.060244	0.72	0.857201	1.76	0.10320	1.61	612	16	629	17	633	19	103
S8 L_12.1_10-25-55	25	249	24	0.061554	0.63	0.945108	1.89	0.11136	1.78	659	14	676	19	681	23	103
S8 L_13.1_10-25-55	25	451	41	0.064369	0.81	0.944863	2.36	0.10646	2.22	754	17	675	23	652	28	87
S8 L_14.1_10-25-55	25	1721	77	0.090818	2.27	0.688446	6.84	0.05498	6.45	1443	43	532	57	345	43	24
S8 L_15.1_10-25-55	25	231	20	0.059324	0.65	0.833028	2.21	0.10184	2.11	579	14	615	20	625	25	108
S8 L_16.1_10-25-55	25	768	93	0.083269	1.28	1.678712	4.90	0.14621	4.73	1276	25	1000	63	880	78	69
S8 L_16.2_10-25-55	25	1496	104	0.089042	1.45	1.066583	6.30	0.08688	6.13	1405	28	737	67	537	63	38
S8 L_17.1_10-25-55	25	164	15	0.061290	0.65	0.888874	1.82	0.10518	1.70	649	14	646	17	645	21	99
S8 L_107.1_10-35-55	35	450	53	0.072019	0.68	1.339644	1.91	0.13491	1.78	986	14	863	22	816	27	83
S8 L_18.1_10-35-55	35	837	72	0.072242	0.79	0.996260	2.01	0.10002	1.85	993	16	702	20	615	22	62
S8 L_19.1_10-35-55	35	100	10	0.073592	1.98	1.098952	2.59	0.10830	1.67	1030	40	753	28	663	21	64
S8 L_20.1_10-35-55	35	82	8	0.071990	2.56	1.060979	3.13	0.10689	1.80	986	52	734	33	655	22	66
S8 L_21.1_10-35-55	35	599	51	0.061037	0.76	0.826210	1.82	0.09817	1.66	641	16	612	17	604	19	94
S8 L_22.1_10-35-55	35	239	22	0.061822	0.67	0.895715	1.71	0.10508	1.57	668	14	649	16	644	19	96
S8 L_23.1_10-35-55	35	787	77	0.079767	0.59	1.222759	1.76	0.11118	1.65	1191	12	811	20	680	21	57
S8 L_24.1_10-35-55	35	308	45	0.071891	0.61	1.654017	1.73	0.16687	1.62	983	12	991	22	995	30	101
S8 L_25.1_10-35-55	35	316	33	0.093328	4.85	1.504712	5.15	0.11693	1.73	1495	92	932	64	713	23	48
S8 L_26.1_10-35-55	35	522	39	0.068184	2.41	0.825132	4.41	0.08777	3.69	874	50	611	41	542	38	62
S8 L_27.1_10-35-55	35	251	22	0.060531	0.70	0.856346	1.81	0.10260	1.68	623	15	628	17	630	20	101
S8 L_28.1_10-35-55	35	140	15	0.065624	0.77	1.092754	1.76	0.12077	1.58	794	16	750	19	735	22	93
S8 L_29.1_10-35-55	35	401	29	0.067829	0.86	0.764344	3.16	0.08173	3.04	863	18	577	28	506	30	59
S8 L_30.1_10-35-55	35	645	42	0.074644	1.95	0.762653	2.99	0.07410	2.27	1059	39	576	26	461	20	44
S8 S_1.1_10-25-55	25	227	19	0.060622	0.60	0.835128	1.60	0.09991	1.48	626	13	616	15	614	17	98
S8 S_2.1_10-25-55	25	879	51	0.072128	0.63	0.684402	2.36	0.06882	2.27	990	13	529	20	429	19	43
S8 S_3.1_10-25-55	25	431	106	0.121372	0.64	4.630761	1.75	0.27671	1.63	1976	11	1755	29	1575	46	80
S8 S_4.1_10-25-55	25	159	22	0.072275	0.59	1.653470	1.56	0.16592	1.44	994	12	991	20	990	26	100
S8 S_5.1_10-25-55	25	1070	71	0.085696	5.04	0.930227	5.55	0.07873	2.32	1331	98	668	55	489	22	37
S8 S_6.1_10-25-55	25	963	189	0.125981	0.62	4.049742	5.72	0.23314	5.68	2043	11	1644	95	1351	139	66
S8 S_7.1_10-25-55	25	635	68	0.079441	0.85	1.391955	2.62	0.12708	2.48	1183	17	886	31	771	36	65
S8 S_8.1_10-25-55	25	438</														

Table 6

sample	spot	U	Pb	ratios												conc.
				Ø	[ppm]	[ppm]	$^{207}\text{Pb}/^{206}\text{Pb}$	1σ	$^{207}\text{Pb}/^{235}\text{U}$	1σ	$^{206}\text{Pb}/^{238}\text{U}$	1σ	$^{207}\text{Pb}/^{206}\text{Pb}$	2σ	$^{207}\text{Pb}/^{235}\text{U}$	2σ
D600L_1.1_10-35-55	35	432	45	0.063356	0.67	1.071062	1.97	0.12261	1.86	720	14	739	21	746	26	104
D600L_2.1_10-35-55	35	172	23	0.069609	0.68	1.499854	2.00	0.15627	1.88	917	14	930	25	936	33	102
D600L_3.1_10-35-55	35	1333	282	0.176065	0.70	5.477466	2.95	0.22563	2.87	2616	12	1897	51	1312	68	50
D600L_3.2_10-35-55	35	2010	251	0.192177	1.41	3.581073	5.86	0.13515	5.68	2761	23	1545	95	817	88	30
D600L_4.1_10-35-55	35	504	219	0.170895	0.66	10.862712	2.11	0.46101	2.00	2566	11	2511	40	2444	82	95
D600L_5.1_10-35-55	35	165	16	0.075871	0.97	1.135610	2.34	0.10856	2.13	1092	19	770	25	664	27	61
D600L_5.2_10-25-55	25	69	17	0.146236	0.99	5.359337	3.84	0.26580	3.71	2302	17	1878	67	1519	101	66
D600L_6.1_10-35-55	35	118	10	0.061297	0.75	0.831656	2.07	0.09840	1.93	650	16	615	19	605	22	93
D600L_7.1_10-35-55	35	381	159	0.169525	0.68	10.353507	2.07	0.44295	1.95	2553	11	2467	39	2364	77	93
D600L_8.1_10-35-55	35	563	38	0.072828	1.77	0.780527	2.62	0.07773	1.94	1009	36	586	23	483	18	48
D600L_8.2_10-35-55	35	220	16	0.057607	0.67	0.667750	2.01	0.08407	1.90	515	15	519	16	520	19	101
D600L_9.1_10-35-55	35	160	20	0.068824	0.94	1.383568	2.33	0.14580	2.13	893	19	882	28	877	35	98
D600L_9.2_10-35-55	35	258	30	0.066976	0.99	1.243338	2.87	0.13464	2.70	837	21	820	33	814	41	97
D600L_10.1_10-35-55	35	705	56	0.058945	0.68	0.753522	2.00	0.09271	1.89	565	15	570	18	572	21	101
D600L_11.1_10-35-55	35	141	60	0.162296	0.68	10.091272	2.36	0.45096	2.26	2480	12	2443	44	2400	91	97
D600L_12.1_10-35-55	35	79	11	0.072603	0.76	1.604500	2.13	0.16028	1.98	1003	15	972	27	958	35	96
D600L_13.1_10-35-55	35	155	22	0.071601	0.70	1.633895	2.09	0.16550	1.97	975	14	983	26	987	36	101
D600L_14.1_10-35-55	35	131	10	0.060500	0.74	0.738092	2.09	0.08848	1.96	621	16	561	18	547	21	88
D600L_15.1_10-35-55	35	279	51	0.077787	0.69	2.244404	2.10	0.20926	1.99	1141	14	1195	30	1225	44	107
D600L_16.1_10-35-55	35	371	37	0.062226	0.68	0.990845	2.05	0.11549	1.93	682	15	699	21	705	26	103
D600L_17.1_10-35-55	35	112	9	0.060875	0.77	0.826335	2.07	0.09845	1.93	635	17	612	19	605	22	95
D600L_18.1_10-35-55	35	158	38	0.096000	0.68	3.671162	2.02	0.27735	1.90	1548	13	1565	32	1578	53	102
D600L_19.1_10-35-55	35	206	29	0.072277	0.70	1.616419	2.06	0.16220	1.94	994	14	977	26	969	35	98
D600L_20.1_10-35-55	35	49	7	0.072628	0.80	1.696586	2.15	0.16942	2.00	1004	16	1007	28	1009	37	101
D600L_21.1_10-35-55	35	238	82	0.128279	0.67	6.665042	2.04	0.37683	1.93	2075	12	2068	36	2061	68	99
D600L_22.1_10-35-55	35	378	32	0.059960	0.68	0.812024	2.01	0.09822	1.89	602	15	604	18	604	22	100
D600L_23.1_10-35-55	35	255	36	0.070986	0.68	1.611140	2.01	0.16461	1.90	957	14	975	25	982	35	103
D600L_24.1_10-35-55	35	121	14	0.066573	0.73	1.286607	2.04	0.14017	1.90	824	15	840	23	846	30	103
D600L_25.1_10-35-55	35	903	246	0.170331	0.67	6.720672	2.63	0.28617	2.55	2561	11	2075	47	1622	73	63
D600L_25.2_10-25-55	25	621	182	0.170493	0.69	7.336132	2.29	0.31208	2.19	2562	12	2153	41	1751	67	68
D600L_26.1_10-35-55	35	58	9	0.071668	0.74	1.622780	2.30	0.16422	2.18	977	15	979	29	980	40	100
D600L_27.1_10-35-55	35	394	36	0.061159	0.73	0.903714	2.01	0.10717	1.87	645	16	654	19	656	23	102
D600L_28.1_10-35-55	35	189	59	0.113879	0.68	5.409246	2.05	0.34450	1.93	1862	12	1886	35	1908	64	102
D600L_29.1_10-35-55	35	124	18	0.071687	0.70	1.672801	2.02	0.16924	1.89	977	14	998	26	1008	35	103
D600L_30.1_10-35-55	35	42	5	0.068763	0.77	1.310032	2.17	0.13817	2.03	892	16	850	25	834	32	94
D600L_31.1_10-35-55	35	239	21	0.060395	0.70	0.862927	2.11	0.10363	1.99	618	15	632	20	636	24	103
D600L_32.1_10-35-55	35	165	17	0.063767	0.71	1.073296	2.02	0.12207	1.89	734	15	740	21	742	27	101
D600L_33.1_10-35-55	35	538	52	0.063977	0.70	0.992117	2.02	0.11247	1.89	741	15	700	20	687	25	93
D600L_34.1_10-35-55	35	39	5	0.070503	0.75	1.492314	2.27	0.15351	2.14	943	15	927	28	921	37	98
D600L_35.1_10-35-55	35	155	51	0.121007	0.69	6.048741	2.06	0.36254	1.94	1971	12	1983	36	1994	67	101
D600L_36.1_10-35-55	35	282	87	0.120523	0.75	5.606095	2.									

Table 7

sample	spot	U	Pb	ratios												conc.
				Ø	[ppm]	[ppm]	$^{207}\text{Pb}/^{206}\text{Pb}$	1σ	$^{207}\text{Pb}/^{235}\text{U}$	1σ	$^{206}\text{Pb}/^{238}\text{U}$	1σ	$^{207}\text{Pb}/^{206}\text{Pb}$	2σ	$^{207}\text{Pb}/^{235}\text{U}$	2σ
D470L_1.1_10-35-55	35	69	10	0.074645	1.52	1.676141	1.70	0.16286	0.76	1059	31	1000	22	973	14	92
D470L_2.1_10-35-55	35	110	11	0.064408	1.25	1.034282	1.53	0.11647	0.88	755	26	721	16	710	12	94
D470L_3.1_10-35-55	35	193	17	0.061740	1.20	0.891279	1.42	0.10470	0.76	665	26	647	14	642	9	97
D470L_4.1_10-35-55	35	132	38	0.109322	1.18	4.793333	1.50	0.31800	0.92	1788	22	1784	25	1780	29	100
D470L_5.1_10-35-55	35	298	24	0.059941	1.22	0.773851	1.55	0.09363	0.96	601	26	582	14	577	11	96
D470L_6.1_10-35-55	35	175	17	0.063249	1.20	0.994829	1.41	0.11408	0.74	717	25	701	14	696	10	97
D470L_8.1_10-35-55	35	355	67	0.083116	1.18	2.467578	1.38	0.21532	0.72	1272	23	1263	20	1257	17	99
D470L_9.1_10-35-55	35	168	15	0.077424	1.73	1.075048	1.94	0.10070	0.88	1132	34	741	21	619	10	55
D470L_10.1_10-35-55	35	63	6	0.063110	1.41	0.950408	1.69	0.10922	0.94	712	30	678	17	668	12	94
D470L_11.1_10-35-55	35	119	18	0.071908	1.24	1.694605	1.43	0.17092	0.73	983	25	1007	18	1017	14	103
D470L_12.1_10-35-55	35	91	8	0.061668	1.34	0.839793	1.54	0.09877	0.76	663	29	619	14	607	9	92
D470L_13.1_10-35-55	35	185	18	0.063250	1.32	0.966748	1.52	0.11085	0.75	717	28	687	15	678	10	95
D470L_14.1_10-35-55	35	89	8	0.064214	2.34	0.895174	2.50	0.10111	0.91	749	49	649	24	621	11	83
D470L_15.1_10-35-55	35	58	5	0.060362	1.40	0.780138	1.59	0.09374	0.76	617	30	586	14	578	8	94
D470L_16.1_10-35-55	35	49	4	0.061430	1.58	0.783012	1.75	0.09245	0.75	654	34	587	16	570	8	87
D470L_17.2_10-25-55	25	63	2	0.051011	5.57	0.266404	5.73	0.03788	1.37	241	128	240	25	240	6	99
D470L_18.1_10-35-55	35	516	41	0.058301	0.95	0.756842	1.53	0.09415	1.20	541	21	572	13	580	13	107
D470L_19.1_10-35-55	35	920	88	0.062573	0.97	0.988991	1.62	0.11463	1.30	694	21	698	16	700	17	101
D470L_20.1_10-35-55	35	590	22	0.052825	1.11	0.330436	1.63	0.04537	1.19	321	25	290	8	286	7	89
D470L_21.1_10-35-55	35	132	44	0.120527	0.93	6.245480	1.62	0.37582	1.32	1964	17	2011	28	2057	47	105
D470L_22.1_10-35-55	35	464	38	0.058651	0.94	0.793745	1.56	0.09815	1.24	554	21	593	14	604	14	109
D470L_23.1_10-35-55	35	148	12	0.061570	1.07	0.835682	1.69	0.09844	1.31	659	23	617	16	605	15	92
D470L_24.1_10-35-55	35	387	35	0.060115	1.00	0.903274	1.63	0.10898	1.29	608	22	653	16	667	16	110
D470L_25.1_10-35-55	35	667	69	0.063409	0.94	1.074665	1.63	0.12292	1.33	722	20	741	17	747	19	104
D470L_26.1_10-35-55	35	278	23	0.058601	1.02	0.805872	1.61	0.09974	1.25	552	22	600	15	613	15	111
D470L_27.1_10-35-55	35	252	37	0.071664	0.95	1.704956	1.75	0.17255	1.47	976	19	1010	23	1026	28	105
D470L_28.1_10-35-55	35	108	10	0.062111	1.07	0.908769	1.68	0.10612	1.30	678	23	656	16	650	16	96
D470L_29.1_10-35-55	35	155	16	0.063496	0.96	1.080800	1.77	0.12345	1.49	725	20	744	19	750	21	104
D470L_30.1_10-35-55	35	372	34	0.081658	1.13	1.194011	1.74	0.10605	1.32	1237	22	798	19	650	16	53
D470L_31.1_10-35-55	35	204	26	0.068513	0.94	1.409045	1.55	0.14916	1.23	884	19	893	18	896	21	101
D470L_32.1_10-35-55	35	1881	327	0.174933	0.94	4.418893	1.79	0.18321	1.52	2605	16	1716	30	1084	30	42
D470L_32.2_10-35-55	35	1905	340	0.169889	0.94	4.440462	1.88	0.18957	1.63	2557	16	1720	31	1119	34	44
D470L_33.1_10-35-55	35	75	11	0.069328	1.04	1.612438	1.68	0.16868	1.32	909	21	975	21	1005	25	111
D470L_34.1_10-35-55	35	121	20	0.075988	0.98	2.019754	1.58	0.19277	1.23	1095	20	1122	22	1136	26	104
D470L_35.1_10-35-55	35	187	63	0.121210	0.94	6.221460	1.57	0.37227	1.26	1974	17	2007	28	2040	44	103
D470L_36.1_10-35-55	35	503	46	0.061647	0.96	0.895812	1.53	0.10539	1.20	662	21	649	15	646	15	98
D470L_37.1_10-35-55	35	20	2	0.079614	2.44	1.325250	2.73	0.12073	1.23	1187	48	857	32	735	17	62
D470L_38.1_10-35-55	35	240	24	0.064847	0.96	1.043370	1.56	0.11669	1.23	769	20	726	16	712	17	92
D470L_39.1_10-35-55	35	1690	257	0.181116	1.24	4.012798	5.85	0.16069	5.72	2663	21	1637	97	961	103	36
D470L_40.1_10-35-55	35	1138	311	0.181336	0.95	7.160021	2.84	0.28637	2.68	2665	16	2132	51	1623	77	61
D470L_41.1_10-35-55	35	357	129	0.128682	0.95	7.054161	1.59	0.39758	1.							

Table 8

sample	spot	U	Pb	ratios												conc.
				Ø	[ppm]	[ppm]	$^{207}\text{Pb}/^{206}\text{Pb}$	1σ	$^{207}\text{Pb}/^{235}\text{U}$	1σ	$^{206}\text{Pb}/^{238}\text{U}$	1σ	$^{207}\text{Pb}/^{206}\text{Pb}$	2σ	$^{207}\text{Pb}/^{235}\text{U}$	2σ
01WP19_10-35-50	35	199	16	0.06016	0.865929	0.78501	1.366175	0.09464	1.056693	609	37	588	12	583	12	96
02WP19_10-35-50	35	57	8	0.07360	0.863175	1.66703	1.311009	0.16427	0.98675	1030	35	996	17	980	18	95
03WP19_10-35-50	35	393	113	0.10840	0.803599	4.67879	1.181829	0.31304	0.866573	1773	29	1763	20	1756	27	99
04WP19_10-35-50	35	316	32	0.06326	0.813397	1.01048	1.19925	0.11586	0.881241	717	35	709	12	707	12	99
05WP19_10-35-50	35	434	36	0.06011	0.816779	0.80276	1.285921	0.09686	0.99321	607	35	598	12	596	11	98
06WP19_10-35-50	35	86	7	0.05978	0.866318	0.79055	1.434852	0.09592	1.143807	596	37	591	13	590	13	99
07WP19_10-35-50	35	84	7	0.05981	0.933839	0.79489	1.40474	0.09639	1.049399	597	40	594	13	593	12	99
08WP19_10-35-50	35	212	18	0.06150	0.831595	0.86558	1.239844	0.10208	0.9196	657	36	633	12	627	11	95
09WP19_10-35-50	35	329	110	0.12982	0.809438	6.50536	1.533368	0.36344	1.302316	2095	28	2047	27	1998	45	95
10WP19_10-35-50	35	526	31	0.05472	0.817479	0.51494	1.312	0.06826	1.026193	401	37	422	9	426	8	106
11WP19_10-35-50	35	986	94	0.06196	0.805689	0.93704	1.251943	0.10968	0.958241	673	35	671	12	671	12	100
12WP19_10-35-50	35	153	46	0.11373	0.806939	5.31475	1.325618	0.33892	1.05172	1860	29	1871	23	1881	34	101
13WP19_10-35-50	35	266	27	0.06318	0.826036	1.02368	1.203103	0.11751	0.874713	714	35	716	12	716	12	100
14WP19_10-35-50	35	167	24	0.07286	0.850017	1.66158	1.345499	0.16539	1.042994	1010	34	994	17	987	19	98
15WP19_10-35-50	35	478	13	0.05138	0.857846	0.22792	1.378792	0.03217	1.07943	258	39	208	5	204	4	79
16WP19_10-35-50	35	561	43	0.05912	0.814965	0.71797	1.292567	0.08807	1.003275	572	35	549	11	544	10	95
16bWP19_10-35-50	35	638	49	0.05876	0.821614	0.73680	1.273838	0.09095	0.973455	558	36	561	11	561	10	101
17WP19_10-35-50	35	135	20	0.07246	0.816963	1.68599	1.438828	0.16876	1.184398	999	33	1003	18	1005	22	101
18WP19_10-25-50	25	697	68	0.12500	0.807802	1.74112	1.724183	0.10102	1.523241	2029	29	1024	22	620	18	31
19WP19_10-35-50	35	52	8	0.07338	0.832473	1.74050	1.642493	0.17203	1.4159	1024	34	1024	21	1023	26	100
20WP19_10-35-50	35	209	81	0.13879	0.802581	7.92868	1.429283	0.41432	1.182672	2212	28	2223	26	2235	45	101
21WP19_10-35-50	35	204	31	0.07373	0.816387	1.73175	1.391995	0.17035	1.127459	1034	33	1020	18	1014	21	98
22WP19_10-35-50	35	225	19	0.06022	0.820485	0.79858	1.419086	0.09618	1.157847	612	35	596	13	592	13	97
23WP19_10-35-50	35	734	58	0.06477	0.841961	0.81205	1.970996	0.09094	1.782113	767	35	604	18	561	19	73
24WP19_10-25-50	25	268	124	0.18046	0.802319	11.75646	1.407563	0.47250	1.156511	2657	27	2585	27	2495	48	94
25WP19_10-35-50	35	265	41	0.09372	0.911798	2.23339	1.511539	0.17283	1.205559	1503	34	1192	21	1028	23	68
26WP19_10-35-50	35	188	29	0.07408	0.813637	1.79318	1.405279	0.17556	1.145777	1044	33	1043	18	1043	22	100
27WP19_10-35-50	35	125	13	0.06617	0.974778	1.16559	1.562145	0.12775	1.220698	812	41	785	17	775	18	95
28WP19_10-35-50	35	194	63	0.12155	0.801961	6.05768	1.464222	0.36145	1.225073	1979	29	1984	26	1989	42	101
29WP19_10-35-50	35	234	75	0.12510	0.835172	5.99801	1.583318	0.34775	1.345134	2030	30	1976	28	1924	45	95
30WP19_10-35-50	35	168	68	0.17546	0.801571	10.31199	1.416244	0.42625	1.167575	2610	27	2463	26	2289	45	88
31WP19_10-35-50	35	53	30	0.24191	0.920201	18.18887	1.861566	0.54533	1.618227	3133	29	3000	36	2806	74	90
32WP19_10-35-50	35	231	21	0.06120	0.811635	0.88555	1.526611	0.10494	1.292977	646	35	644	15	643	16	100
33WP19_10-35-50	35	182	28	0.07364	0.825524	1.73396	1.586966	0.17077	1.355349	1032	33	1021	21	1016	26	99
34WP19_10-35-50	35	168	13	0.05838	0.850932	0.70624	1.670208	0.08774	1.437188	544	37	543	14	542	15	100
35WP19_10-35-50	35	184	88	0.17715	0.801989	12.10053	1.58936	0.49542	1.372181	2626	27	2612	30	2594	59	99
36WP19_10-50-50	50	20	2	0.06752	0.906452	1.14685	1.518602	0.12320	1.2184	854	38	776	16	749	17	88
37WP19_10-35-50	35	22	3	0.07378	0.948847	1.74314	1.670343	0.17136	1.374677	1035	38	1025	21	1020	25	98
38WP19_10-35-50	35	242	29	0.06741	0.810343	1.29514	1.747786	0.13934	1.54858	851	34	844	20	841	24	99
39WP19_10-35-50	35															

sample	spot	U	Pb	ratios												conc.
				Ø	[ppm]	[ppm]	$^{207}\text{Pb}/^{206}\text{Pb}$	1σ	$^{207}\text{Pb}/^{235}\text{U}$	1σ	$^{206}\text{Pb}/^{238}\text{U}$	1σ	$^{207}\text{Pb}/^{206}\text{Pb}$	2σ	$^{207}\text{Pb}/^{235}\text{U}$	2σ
01WP103sm_10-35-50	35	63	34	0.20007	0.81	14.97042	1.22	0.54268	0.91	2827	26	2813	23	2795	41	99
02WP103sm_10-35-50	35	594	52	0.06042	0.81	0.83539	1.27	0.10028	0.99	619	35	617	12	616	12	100
03WP103sm_10-35-50	35	221	72	0.12113	0.81	5.93093	1.31	0.35510	1.04	1973	29	1966	23	1959	35	99
04WP103sm_10-35-50	35	514	54	0.06378	0.81	1.05971	1.42	0.12050	1.17	734	34	734	15	733	16	100
05WP103sm_10-35-50	35	254	39	0.07462	0.81	1.83428	1.30	0.17827	1.02	1058	33	1058	17	1058	20	100
06WP103sm_10-35-50	35	118	60	0.18654	0.81	13.64560	1.30	0.53054	1.02	2712	27	2725	25	2744	46	101
07WP103sm_10-35-50	35	337	33	0.06289	0.81	0.98926	1.36	0.11409	1.09	704	35	698	14	696	14	99
08bWP103sm_10-25-50	25	63	32	0.19859	0.82	14.41919	1.35	0.52660	1.07	2815	27	2778	26	2727	47	97
09WP103sm_10-35-50	35	570	51	0.06157	0.81	0.90457	1.20	0.10656	0.89	659	35	654	12	653	11	99
10WP103sm_10-35-50	35	419	32	0.05871	0.82	0.72896	1.24	0.09004	0.93	557	36	556	11	556	10	100
11WP103sm_10-35-50	35	142	62	0.16343	0.81	10.42338	1.30	0.46257	1.02	2491	27	2473	24	2451	42	98
12WP103sm_10-35-50	35	126	63	0.18619	0.80	13.55225	1.43	0.52790	1.19	2709	27	2719	27	2733	53	101
13WP103sm_10-35-50	35	55	28	0.18700	0.81	13.50589	1.28	0.52382	0.99	2716	27	2716	24	2715	44	100
14bWP103sm_10-35-50	35	152	49	0.14327	2.84	6.39227	6.39	0.32360	5.73	2267	98	2031	115	1807	182	80
14WP103sm_10-35-50	35	309	147	0.17415	0.80	11.73734	1.32	0.48880	1.05	2598	27	2584	25	2565	45	99
15WP103sm_10-35-50	35	376	35	0.06148	0.81	0.90936	1.29	0.10716	1.01	656	35	656	13	656	13	100
16WP103sm_10-35-50	35	95	49	0.18683	0.80	13.53936	1.33	0.52560	1.06	2714	27	2718	25	2723	47	100
17bWP103sm_10-35-50	35	131	5	0.05416	0.92	0.35586	1.33	0.04766	0.96	378	41	309	7	300	5	79
17cWP103sm_10-35-50	35	114	5	0.05509	0.93	0.36288	1.39	0.04778	1.03	416	41	314	7	301	6	72
17dWP103sm_10-75-50	75	98	4	0.05538	0.81	0.37329	1.26	0.04889	0.96	427	36	322	7	308	6	72
17eWP103sm_10-75-50	75	118	5	0.05491	0.88	0.36353	1.27	0.04802	0.92	409	39	315	7	302	5	74
17WP103sm_10-50-50	50	67	3	0.05514	1.00	0.36915	1.36	0.04856	0.92	418	44	319	7	306	5	73
18WP103sm_10-35-50	35	90	41	0.16996	0.85	11.29713	1.37	0.48207	1.08	2557	29	2548	26	2536	45	99
19WP103sm_10-35-50	35	123	39	0.12189	0.80	6.13563	1.29	0.36508	1.01	1984	29	1995	23	2006	35	101
20WP103sm_10-35-50	35	133	67	0.18686	0.80	13.71868	1.27	0.53248	0.98	2715	26	2730	24	2752	44	101
21WP103sm_10-35-50	35	89	44	0.18794	0.81	13.66140	1.46	0.52719	1.22	2724	27	2727	28	2730	54	100
22WP103sm_10-35-50	35	74	37	0.18708	0.81	13.54329	1.25	0.52504	0.95	2717	27	2718	24	2721	42	100
23bWP103sm_10-25-50	25	247	131	0.18794	0.81	13.86411	1.33	0.53503	1.06	2724	27	2740	25	2763	48	101
23WP103sm_10-25-50	25	388	203	0.18824	0.80	13.61932	1.28	0.52474	1.00	2727	26	2724	24	2719	45	100
24bWP103sm_10-50-50	50	32	16	0.18605	0.80	13.81621	1.27	0.53860	0.98	2708	27	2737	24	2778	44	103
24WP103sm_10-35-50	35	174	89	0.18668	0.80	13.47529	1.37	0.52352	1.11	2713	26	2714	26	2714	49	100
25WP103sm_10-35-50	35	59	30	0.18738	0.81	13.60240	1.31	0.52649	1.03	2719	27	2722	25	2727	46	100
26WP103sm_10-35-50	35	49	25	0.19892	0.82	14.60648	1.49	0.53256	1.24	2817	27	2790	28	2752	55	98
27WP103sm_10-35-50	35	174	17	0.06224	0.82	0.95558	1.37	0.11135	1.09	682	35	681	14	681	14	100
28WP103sm_10-50-50	50	32	12	0.13950	0.81	8.06304	1.42	0.41919	1.17	2221	28	2238	26	2257	45	102
29WP103sm_10-50-50	50	111	59	0.19867	0.80	14.84285	1.31	0.54185	1.04	2815	26	2805	25	2791	48	99
30WP103sm_10-35-50	35	141	75	0.20408	0.80	15.43298	1.25	0.54847	0.96	2859	26	2842	24	2819	44	99
31WP103L_10-50-50	50	38	19	0.18573	0.80	13.57669	1.36	0.53017	1.09	2705	26	2721	26	2742	49	101
32WP103L_10-75-50	75	70	5	0.06451	1.44	0.78070	1.72	0.08777	0.95	759	61	586	15	542	10	71
33bWP103L_10-25-50	25	165	73	0.17369	0.80	11.01570	1.26	0.45997	0.96	2594	27	2524	24	2439	39	94
33WP103L_10-75-50	35	68	30	0.16784	0.83	10.71807	1.46	0.46314	1.21	2536	28	2499	27	2453	49	97
34WP103L_10-35-50																